Heliyon 6 (2020) e05397

Contents lists available at ScienceDirect

Heliyon

journal homepage: www.cell.com/heliyon

Research article

A cell model in the ventral visual pathway for the detection of circles of curvature constituting figures

Susumu Kawakami [a,*], Takehiro Ito [a], Yoshinari Makino [a,b], Makoto Hashimoto [a], Masafumi Yano [a,c]

[a] Tohoku University, Research Institute of Electrical Communication, 2-1-1 Katahira, Aoba-ku, Sendai 980-8577, Japan
[b] Tohoku Gakuin University, Department of Information Science, Faculty of Liberal Arts, 2-1-1 Tenjinzawa, Izumi-ku, Sendai 981-3193, Japan
[c] Tohoku Institute of Technology, 35-1 Yagiyamakasumichou, Taihaku-ku, Sendai 982-8577, Japan

ARTICLE INFO

Keywords:
Cell model
Curvature-circle detection
3D normal-line transform
Column
Coarse-to-fine extraction
Cell-array conversion
Shape recognition
Information systems
Behavioral neuroscience
Nervous system
Cognition
Consciousness
Emotion
Systems neuroscience
Mathematical biosciences

ABSTRACT

The contour of an arbitrary figure can be represented as a group of circles of curvature in contact with it, with each curvature circle represented by its center O_C and radius r. We propose a series of cell models for detecting this circle, which is composed of a lateral geniculate nucleus (LGN) cell, nondirectionally selective (NDS) simple cell, and curvature-circle detection cell (CDC). The LGN and NDS simple cells were previously modeled. The CDC has been modeled as follows. Each tangent in contact with this circle is detected by an NDS simple cell that performs the Hough transformation of LGN cell responses, and then this tangent is transformed to a three-dimensional (3D) normal line in a CDC column. This transformation has been named a 3D normal-line transform. Performing this transformation for all tangents causes a CDC at the intersection of these normal lines to fire most intensively, and thus the O_C and r of the circle is detected as the coordinates of this intersection. Therefore, the CDC has been modeled as this 3D normal-line transform. Based on this CDC, we model two types of constancy CDC: a position-invariant CDC and a curvature-invariant CDC. These three types of CDC reflect the response to various stimuli in actual area V4 cells. In order to validate these CDC types neurophysiologically, we propose an experimental method using microelectrodes. Cell models previously reported correspond to this hierarchy: the S1, S2, and C2 cells correspond to the NDS simple cell, CDC, and position-invariant CDC, respectively.

1. Introduction

The purpose of this paper is to model a cell that detects each circle of curvature in contact with the contour of an arbitrary figure (Figure 1(A)) to extract the information (i.e. the center and radius) of the circle. We think that this information may play an important role in shape recognition. To that end, the neurophysiological experiments and cell models reported previously will be investigated and examined as follows.

Shape recognition is thought to be processed in the ventral pathway in primate visual cortex (Felleman and Van Essen 1991; Ungerleider and Mishkin, 1982). At early stages in this pathway, such as the primary visual cortex (V1), shape is processed by cells sensitive to simple features like edge orientation (Hubel & Wiesel, 1959, 1965, 1968). Cells at the end of the pathway in inferotemporal cortex (IT) process abstract object categories like faces and hands (Perrett et al., 1982; Desimone et al., 1984; Fujita et al., 1992; Tanaka et al., 1991; Tsao et al., 2006; Hung et al., 2005; Logothetis et al., 1995). In addition, cells in area IT exhibit an invariance to the translation or size change of a figure (Ito et al., 1995; Tanaka, 1996; Rust and DiCarlo, 2010; Zoccolan et al., 2007). Further, cells in area IT respond in a coarse-to-fine order, specifically, respond first to coarse (or global) components of stimuli and then respond to their fine components with average delay of 51 ms (Sugase et al., 1999; Tamura and Tanaka, 2001). However, the mechanisms of how these abstract object category, invariance, and coarse-to-fine response in area IT are processed by simple features such as edge orientation in area V1 have been not yet understood. In order to approach this issue, it is necessary to elucidate the nature of shape representation at intermediate stages in the ventral pathway such as area V4.

An overview of the various selectivities of area V4 cells to stimuli (i.e. a curvature selectivity, binocular-disparity selectivity, motion-direction selectivity, etc.) was reported (Roe et al., 2012). Since we believe that

* Corresponding author.
E-mail address: RHC02471@nifty.com (S. Kawakami).

https://doi.org/10.1016/j.heliyon.2020.e05397
Received 15 April 2020; Received in revised form 4 July 2020; Accepted 28 October 2020

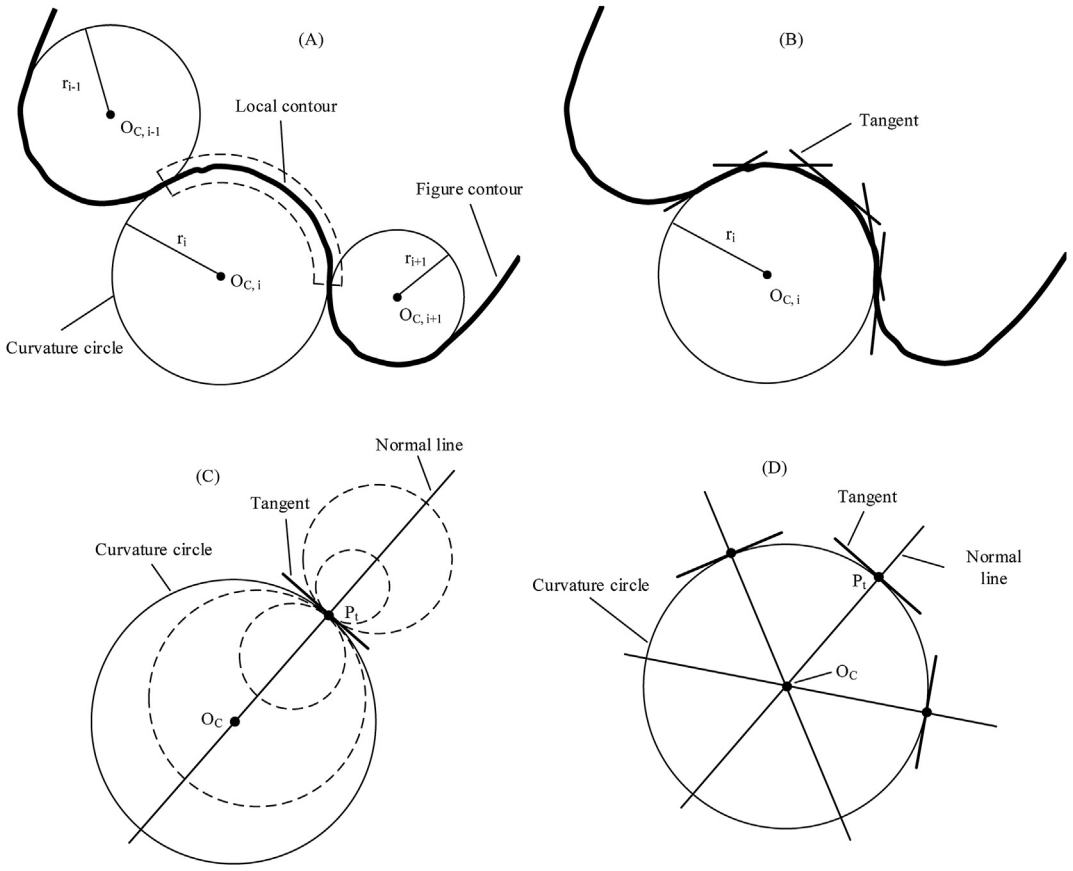

Figure 1. Normal-line transform on a plane. (A) The contour of an arbitrary figure can be represented as a group of curvature circles in contact with the contour, with each curvature circle represented by its center O_C and radius r. (B) One of the curvature circles in (A) is shown. Each tangent in contact with this curvature circle is detected by an NDS simple cell (Kawakami and Okamoto, 1996; Kawakami, 1996). Thus, this detection causes the circle to be converted into an envelope that is composed of all tangents detected by the simple cells. (C) One of the tangents in (B) is shown. This tangent is transformed to a normal line that is perpendicular to it at a contact P_t. This transformation has been named a normal-line transform. The center O_C of every curvature circle (drawn as a dotted line) to should be detected is on this normal line. (D) This normal-line transform converts all tangents of the curvature circle into a group of normal lines that intersect at one point O_C. Thus, the center of the curvature circle is detected as this intersection.

shape recognition is strongly related to curvatures, the following focuses on the curvature selectivity.

Area V4 cells prefer more complex stimuli than edges (Kobatake and Tanaka, 1994) and also prefer curvilinear gratings than linear gratings (Gallant et al., 1993, 1996). In addition, area V4 cells exhibit tuning in both object shape and boundary blur (Oleskiw et al., 2018). Many cells in area V4 respond selectively to the curvature of local contour in a figure. These curvature selectivities can be classified into five types of cell. The first type responds invariant to the position of the contour but selectively to its curvature (Pasupathy & Conner, 1999, 2001, 2002). The second type responds invariant to its size (i.e. its curvature) but selectively to its positions (El-Shamayleh and Pasupathy, 2016). The third type responds selectively to both curvature and position of the contour (El-Shamayleh and Pasupathy, 2016). The fourth type does not respond selectively to a specific curvature but prefers a concentric circle (Gallant et al., 1993, 1996; Dumoulin and Hess, 2007). The fifth type exhibits a trade-off between curvature preferences and position invariances, specifically, exhibits that cells preferring high curvatures have low position invariances, while cells preferring low curvatures have high position invariances (Nandy et al., 2013; Sharpee et al., 2013; Pasupathy and Conner, 1999).

A hierarchy of cell models that respond selectively to the curvature of the local contour was reported (Cadieu et al, 2004, 2007; Riesenhuber and Poggio, 1999; Schneider and Riesenhuber, 2002; Serre et al., 2007). This hierarchy was composed of S1, C1, S2, and C2 cells. The S1 and C1 cells correspond to the simple and complex cells in area V1, respectively. The S2 and C2 cells correspond to the third and first cell types described above, respectively. In addition, a cell model that respond selectively to a very local curvature (i.e. a circular arc with very small central angle) was reported (Rodriguez-Sanchez and Tsotsos, 2012). These cells were combined to model a cell that corresponds to the third type.

Each local contour of a curved figure has been used as a stimulus for the neurophysiological experiments and cell models that were described above. This contour was represented by the parameters (i.e. the position and curvature κ) of it, and the selectivity and invariance of a cell to the contour were evaluated using these parameters. On the other hand, as such parameters, we use the center O_C and radius r of the circle of curvature in contact with this contour (Figure 1(A)): this is because our purpose is to model a cell that detects this circle. The former and latter parameter representations have been respectively named a contour-position representation (which is represented by the position and curvature κ of the contour) and a curvature-center representation (which is represented by the center O_C and radius r of this curvature circle). From the simplicity of the description, we will hereinafter refer to the circle of curvature, the radius of curvature, and the center of curvature as the curvature circle, the curvature radius, and the curvature center, respectively.

Let us compare these parameter representations, in terms of the selectivity evaluation of a cell to the parameters. Since there is a relationship of $\kappa = 1/r$ between the curvature κ and the curvature radius r, they correspond to each other in terms of the selectivity evaluation to them. Next, examine the other parameter, namely the position of the contour, using Figure 1(A). Consider a circle in contact with the contour,

whose center is O_C. When this center O_C changes, the contour position changes correspondingly: that is, they change together. Thus, using either the contour position or the center O_C, the position selectivity of a cell can be evaluated. Therefore, this position corresponds to the center O_C in terms of the selectivity evaluation to them.

To summarize the relationship between these parameters, the curvature κ and position of the contour correspond to the radius r and center O_C of the curvature circle in contact with this contour, respectively. Thus, we can use either of these two representations to evaluate the selectivity of a cell to the parameters. For example, a cell that responds selectively to the position (or curvature κ) of a contour also responds selectively to the center O_C (or radius r) of the curvature circle in contact with this contour, respectively. These correspondences for selectivity are also valid for invariance.

However, the accuracy of position determination differs between these representations, as follows. In the contour-position representation, we can not know which point on the local contour represents the contour position (Figure 1(A)): that is, a reference point that represents the contour position cannot be defined. Although it can be mathematically considered to use the midpoint of the contour as this reference point, cells that determine this midpoint have never been reported as far as we know. Thus, it is physiologically difficult to accurately determine the contour position, because the reference point can not be defined.

On the other hand, in the curvature-center representation, a reference point that represents the contour position can be defined as the center O_C of the curvature circle in contact with the contour (Figure 1(A)), because the position corresponds to this center O_C. Thus, the contour position can be accurately determined as the position of this center O_C. This representation allows the local contour to be defined exactly as one point (O_C,r) in a three-dimensional (3D) space, and thus its parameters (i.e. its center O_C and radius r) can be determined as the coordinates of this point: an algorithm described later uses this 3D space.

Summarize the determination of the curvature and position by these representations as follows. The contour-position representation can determine the curvature κ of the local contour, but is difficult to accurately determine its position. On the other hand, the curvature-center representation allows both radius r and center O_C of the curvature circle (which correspond to the curvature κ and position respectively) to be accurately determined.

In order to achieve physiologically this curvature-center representation, it is necessary to model a cell that detects these parameters (i.e. the center O_C and radius r) of the curvature circle. The above S2 cell (which responds selectively to both curvature κ and position and belongs to the contour-position representation) detects the radius r corresponding to the curvature κ, but is considered to be difficult to accurately detect the center O_C corresponding to the contour position, for the above reason. In addition, an engineering method (Duda and Hart, 1972; Illingworth and Kittler, 1987) for the detection of these parameters was reported, but this method has not been modeled as a cell. In this way, as far as we know, no cell model has been reported that can detect accurately these parameters of the curvature circle.

Therefore, in order to achieve this representation, we proposed a series of cell models that can detect accurately these parameters of the circle. This series was composed of three types of cell model: a lateral geniculate nucleus (LGN) cell, nondirectionally selective (NDS) simple cell, and curvature-circle detection cell (CDC). The LGN and NDS simple cells were previously modeled (Kawakami and Okamoto, 1996; Kawakami, 1996). This CDC was modeled as a 3D normal-line transformation of NDS simple cell responses to detect the parameters (i.e. the O_C and r) of the circle. Computer simulations confirm that this CDC can accurately detect these parameters of any curvature circle.

Based on this CDC, we also modeled two types of constancy CDC that have perceptual constancy: a position-invariant CDC and a curvature-invariant (i.e. size-invariant) CDC. These three types of CDC reflect the response to various stimuli in actual area V4 cells: specifically, these CDC types allow the response of the five cell types in area V4 described above to be explained neurophysiologically. In order to validate these CDC types neurophysiologically, we proposed three types of experimental method using microelectrodes.

Combining these two constancy CDC types with the above series of cell models, we proposed a cell hierarchy that is composed of a series of cell models: the LGN cell, NDS simple cell, CDC, position-invariant CDC, and curvature-invariant CDC.

The previous hierarchy of cell models (Cadieu et al., 2007) described above corresponds to our hierarchy, as follows: that is, the S1, S2, and C2 cells correspond to the NDS simple cell, CDC, and position-invariant CDC, respectively.

Some parts of the material in this paper–the method and cell model for detecting curvature circles, and some computer simulations–have been presented previously (Ito, 2011; Hashimoto, 2009).

2. Algorithm

As shown Figure 1(A), a figure contour can be represented as a group of curvature circles in contact with it: each curvature circle is represented by its center O_C and radius r. This representation, which belongs to the curvature-center representation in Section 1, allows the contour composed of points to be converted into a set of the centers O_C and radii r of these curvature circles: a curve constituted by this set is the evolute of the contour (Bronshtein and Semendyayev, 1978), and this conversion is similar to Fourier transform. To achieve this conversion, we will propose an algorithm for detecting this curvature circle based on the following neurophysiological reports.

An NDS simple cell in area V1 detects each line segment in a local region on the eyeball (i.e. a receptive field (RF)) (Hubel & Wiesel, 1959, 1962; Schiller et al., 1976; Wörgötter and Eysel, 1989), and was modeled as the Hough transformation of LGN cell responses (Kawakami and Okamoto, 1996; Kawakami, 1996): these modeled cells reflect the response to various stimuli in actual NDS simple cells (Kawakami and Okamoto, 1996; Kawakami, 1996; Blasdel, 1992; Okamoto et al., 1999). Based on this line-segment detection, the algorithm for detecting the circles will be described below.

2.1. Detection on a plane

One of the curvature circles in Figure 1(A) is shown in Figure 1(B). Each tangent (i.e. each line segment) in contact with this circle can be detected by an NDS simple cell, as described above. Thus, this detection causes the circle to be to converted into an envelope composed of all tangents: an example of this conversion by modeled NDS simple cells was shown in Figure 7(A)(ii) of Kawakami and Okamoto (1996). This conversion of the circle into the envelope plays an important role in the circle detection, as described below.

One of the tangents in Figure 1(B) is shown in Figure 1(C). Transform this tangent to a normal line that is perpendicular to it at a contact P_t. The transformation from the tangent to this normal line has been named a normal-line transform: the center of every curvature circle (drawn as a dotted line) in contact with this tangent is on the normal line. As shown in Figure 1(D), performing this transformation for all tangents of the circle causes these normal lines to intersect at one point O_C, and thus the center of the circle is detected as this intersection. However, there are two problems as follows: (1) its radius r can not be detected; (2) each of the circles that make up a concentric circle results in the same intersection, and thus can not be detected separately.

In order to solve these problems, we introduce a rectangular solid (x,y,r) shown in Figure 2(A), whose height coordinate is equal to the radius r of a curvature circle to should be detected. The tangent (Figure 1(C)) is transformed to a straight line in this solid, which is expressed by the following equation.

$$y - y_t = (x - x_t)\tan\theta \quad (1)$$

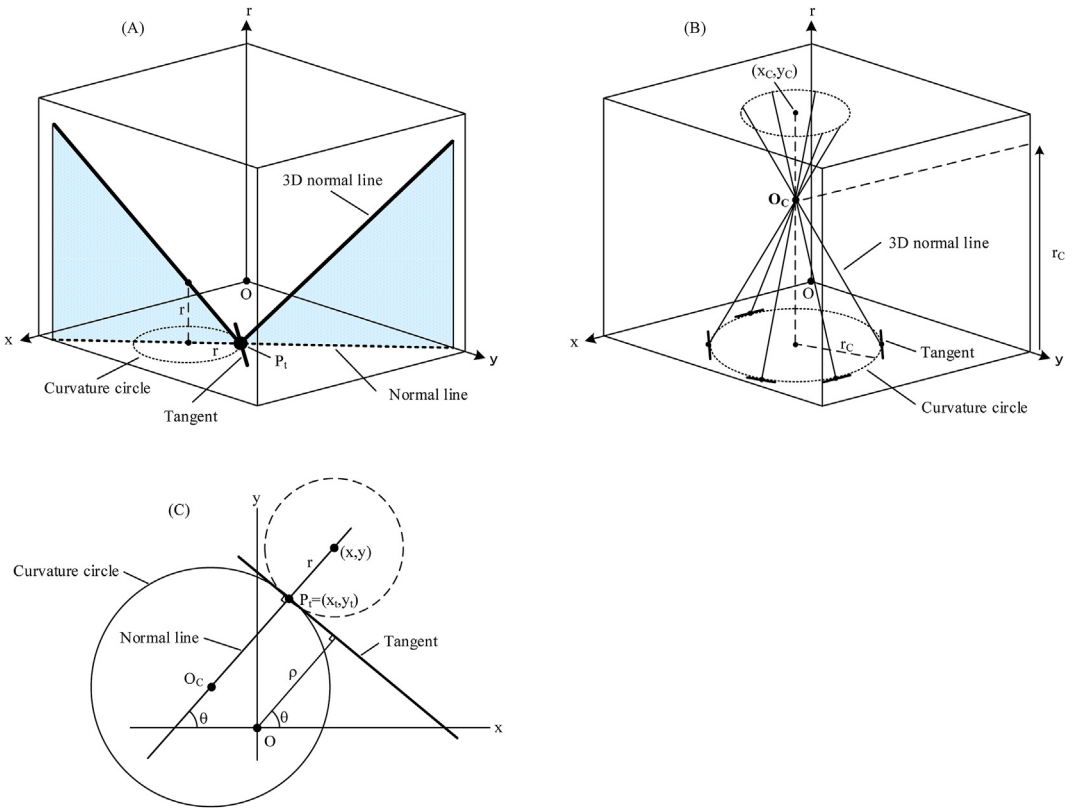

Figure 2. 3D normal-line transform in a rectangular solid. (A) We introduce a rectangular solid (x,y,r) whose height coordinate is equal to the radius r of a curvature circle to should be detected. A tangent in Figure 1(C) is transformed to a 3D normal line in this solid, which is expressed by Eqs. (1) and (2). This transformation has been named a 3D normal-line transform. The curvature circle and normal line corresponding to Figure 1(C) are drawn as dotted lines on the bottom, for reference. (B) This 3D normal-line transform converts all tangents of the curvature circle (Figure 1(D)) into a group of 3D normal lines in the solid (x,y,r). These lines intersect at one point $\mathbf{O_C}$, and thus the center (x_C,y_C) and radius r_C of the circle are detected as the coordinates of this intersection. (C) The tangent in Figure 1(C) is shown which is in contact with the curvature circle. The parameters (ρ,θ) of this tangent are detected by an NDS simple cell (Kawakami and Okamoto, 1996; Kawakami, 1996), where the ρ and θ indicate its location and orientation, respectively.

$$r = \sqrt{((x - x_t)^2 + (y - y_t)^2)} \tag{2}$$

The (x_t,y_t) and θ are the contact P_t and orientation of this tangent (Figure 2(C)), respectively. This straight line has been named a 3D normal line, and the transformation from the tangent to this normal line has been named a 3D normal-line transform. This 3D normal line, which is determined by the tangent's orientation θ and contact (x_t,y_t), is V-shaped because r is a positive value. The bottom of this solid corresponds to the plane shown in Figure 1(C), and a curvature circle and a normal line are drawn on it as dotted lines for reference.

Let us explain how these equations were derived, as follows. A curvature circle and its tangent are shown in Figure 2(C), which corresponds to Figure 1(C). First, the parameters (ρ,θ) of this tangent are detected by an NDS simple cell as described above, where the ρ and θ represent the tangent's location and orientation respectively (Kawakami and Okamoto, 1996; Kawakami, 1996). Next, the normal line perpendicular to this tangent at the contact P_t is expressed by Eq. (1), where (x,y) represents a point on the line. Finally, since the radius r of a curvature circle (drawn as a dotted line in Figure 2(C)) is the distance between (x_t,y_t) and (x,y), the height coordinate r of the 3D normal line is expressed by Eq. (2). Therefore, the 3D normal line has been expressed by Eqs. (1) and (2).

A curvature circle is detected as follows. Each tangent of this circle (Figure 1(D)) is transformed to a 3D normal line in the solid (x,y,r). Then, performing this transformation for all tangents causes these normal lines to intersect at one point $\mathbf{O_C}$ as shown in Figure 2(B), and thus the center (x_C,y_C) and radius r_C of the circle are detected as the coordinates of this intersection: the r height axis is exaggerated for ease of viewing.

Therefore, the above first problem of not being able to detect the radius r has been resolved. In addition, the second problem is solved, as follows: each of the circles that make up a concentric circle can be detected separately, because this circle forms a different intersection at the corresponding height; thus, this problem has been solved. Note that the 3D normal lines outside the contacts are omitted to simplify drawing, and this envelope of the 3D normal lines (Figure 2(B)) forms a right circular cone in the solid.

The above description is summarized. An NDS simple cell detects each tangent in contact with a curvature circle, and then this tangent is transformed into a 3D normal line in the solid (x,y,r). Performing this transformation for all tangents causes these normal lines to intersect at one point, and thus the center and radius of the circle are detected as the coordinates of this intersection.

2.2. Detection on the eyeball

Since the actual scene is projected to the eyeball, an algorithm for detecting a curvature circle on it will be described below. An eyeball viewed from directly above is shown in Figure 3(A): its radius is assumed to be 1.

A curvature circle, whose radius and center are r and $\mathbf{O_C}$ respectively, and a great circle, whose radius and center are π/2 (i.e. 90°) and $\mathbf{O_{C,gr}}$ respectively, are shown on the eyeball. The great circle is the largest circle on the eyeball and is represented by equation (A1) in Appendix A: this circle corresponds to a straight line in space, and can be obtained by projecting this line onto the eyeball. On the other hand, on the plane

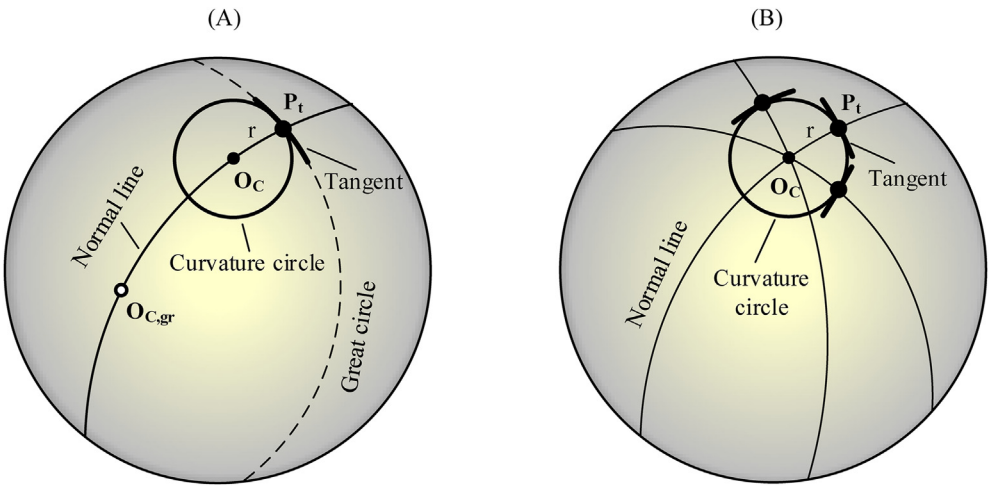

Figure 3. Normal-line transform on the eyeball. (A) A curvature circle and its tangent are shown on the eyeball. This tangent is transformed to a normal line passing through the contact $\mathbf{P_t}$. This transformation is a normal-line transform on the eyeball: the center $\mathbf{O_C}$ of every curvature circle to should be detected is on this normal line. The largest circle on the eyeball is a great circle whose radius and center are $\pi/2$ and $\mathbf{O_{C,gr}}$ respectively. The radius of the eyeball is assumed to be 1. (B) This normal-line transform converts all tangents of the curvature circle into a group of normal lines that intersect at one point $\mathbf{O_C}$. Thus, the center of the circle is detected as this intersection.

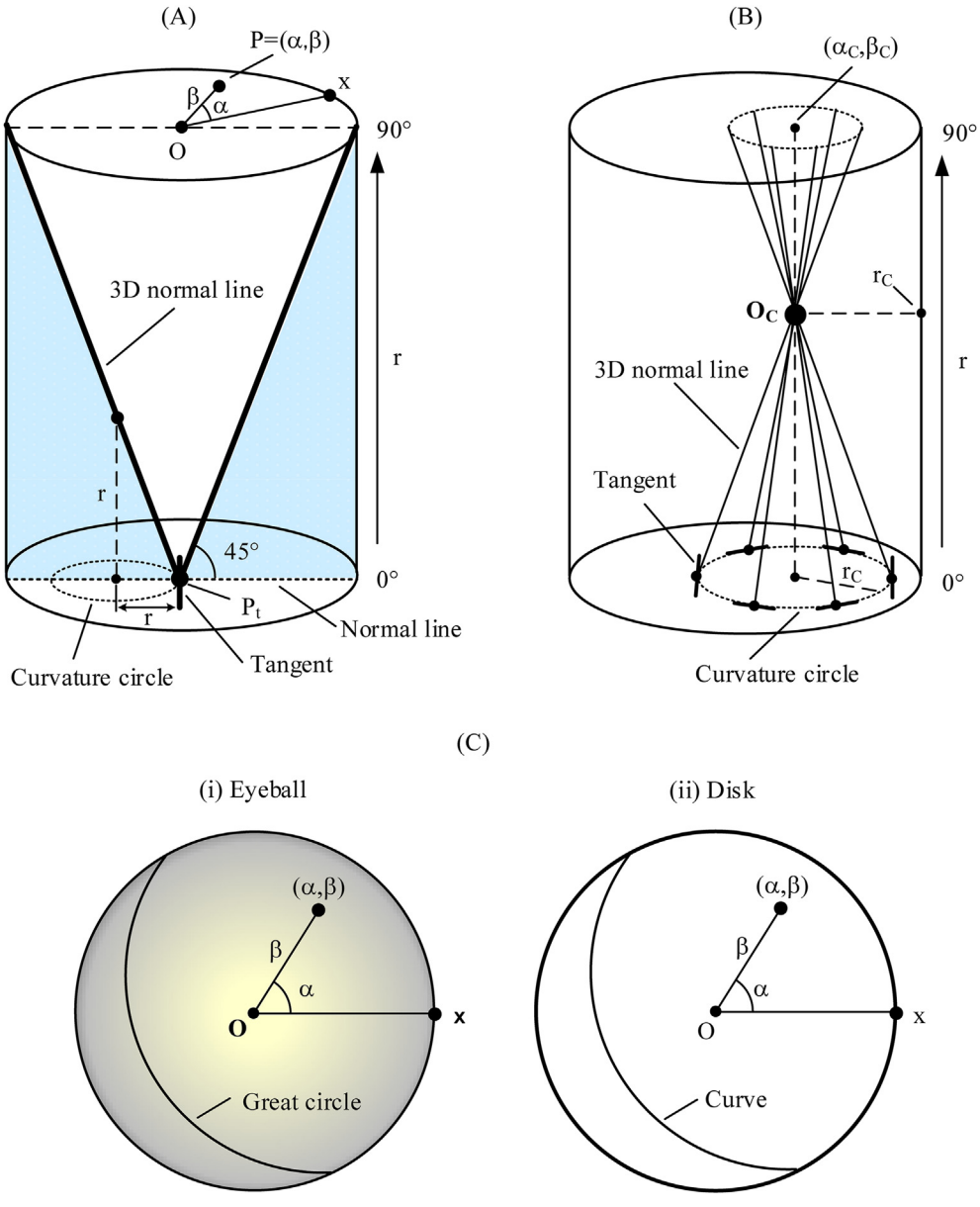

Figure 4. 3D normal-line transform in a cylinder. (A) Instead of the rectangular solid (x,y,r) in Figure 2(A), we introduce a cylinder (α,β,r) whose height coordinate is equal to the radius r of a curvature circle to should be detected. A cross section (α,β) of this cylinder at each height r is obtained as the equidistant projection of the eyeball surface ((C)(i)) onto a disk ((C)(ii)). The tangent on the eyeball (Figure 3(A)) is transformed to a 3D normal line in this cylinder, which is expressed by equations (B3 to B5) in Appendix B. This transformation is a 3D normal-line transform in the cylinder. The curvature circle and normal line corresponding to Figure 3(A) are drawn as dotted lines on the bottom, for reference. The definition of a polar coordinate (α,β) is illustrated in the cross section of r = 90 deg: O corresponds to the center of the visual field, and x represents the x axis. (B) This 3D normal-line transform converts all tangents of the curvature circle (Figure 3(B)) into a group of 3D normal lines in the cylinder (α,β,r). These lines intersect at one point $\mathbf{O_C}$, and thus the center (α_C,β_C) and radius r_C of the circle are detected as the coordinates of this intersection. (C) The equidistant projection of the eyeball surface onto the disk is described, as follows. On the eyeball ((i)), consider a point with the coordinates (α,β) which is represented in polar coordinates: **O** is the center of the visual field. Then, this point is projected to a point on the disk ((ii)) which has the same coordinates (α,β) as on the eyeball. This projection is the equidistant projection of the eyeball surface onto the disk. Note that this projection was used in the previous cell model for detecting a planar surface in space with motion stereo (Kawakami et al., 2000, 2003).

(Section 2.1), the largest circle is a straight line that represents a circle with an infinite radius.

The center of this curvature circle is detected as follows. First, consider a tangent in contact with this circle at a contact $\mathbf{P_t}$ (Figure 3(A)). This tangent (i.e. this line segment) is detected by an NDS simple cell (Section 2.1). Next, transform this tangent to a normal line passing through a contact $\mathbf{P_t}$. This transformation is the normal-line transform on the eyeball. Giving the contact $\mathbf{P_t}$ and the tangent's orientation θ, this normal line is expressed by equation (B3) in Appendix B. Finally, as shown in Figure 3(B), performing this transformation for all tangents of the circle causes these normal lines to intersect at one point $\mathbf{O_C}$, and thus the center of the circle is detected as this intersection $\mathbf{O_C}$.

However, there are two problems as follows: (1) its radius r can not be detected; (2) each of the circles that make up a concentric circle results in the same intersection, and thus can not be detected separately.

2.2.1. 3D normal-line transform in a cylinder

In order to solve these problems, we introduce a cylinder (α,β,r) in Figure 4(A) instead of the solid (x,y,r) in Figure 2(A): a height coordinate of the cylinder is equal to the radius r of a curvature circle to should be detected. A cross section (α,β) of this cylinder at each height is obtained by projecting the eyeball surface in Figure 3(A) onto a disk. This projection is performed as follows.

In Figure 4(C)(i), consider a point with the coordinates (α,β) on the eyeball, which is represented in polar coordinates: **O** is the center of the visual field; when **O** is assumed to be the north pole, α and β correspond to a longitude and a 90° - latitude, respectively. This point is projected to a point on the disk (Figure 4(C)(ii)) which has the same coordinates (α,β) as on the eyeball: the radius of this disk is π/2 that is equal to the distance between **O** and **x** on the eyeball ((i)). This projection has been named an equidistant projection of the eyeball surface onto the disk: this equidistant projection corresponds to one of the projections used to express the characteristics of fisheye lenses. An example of this projection is as follows: a great circle on the eyeball (Figure 4(C)(i)) is projected to a curve on the disk (Figure 4(C)(ii)), and this curve is expressed by equation (A1) in Appendix A.

The cylinder (α,β,r) above has been obtained by stacking these disks (α,β) in the r height direction: the maximum height of this cylinder is π/2 (i.e. 90°), because the largest curvature circle on the eyeball is a great circle. The normal line shown on the bottom as the dotted line is an equidistant projection of the normal line on the eyeball (Figure 3(A)), and is expressed by equations (B3 to B5) in Appendix B.

By adding a height coordinate r to this normal line on the bottom, a 3D normal-line is formed within the cylinder (Figure 4(A)), as follows. Since this height coordinate is equal to the radius r of a curvature circle (shown on the bottom as the dotted line), increasing this radius causes a straight line, which rises in a V shape from the contact P_t at an angle of 45°, to be formed in the cylinder. This V-shaped line is the 3D normal line in the cylinder: the r height axis is exaggerated for ease of viewing. Giving the θ orientation of a tangent and a contact P_t, this 3D normal line is expressed by equations (B3 to B5) in Appendix B.

Thus, the tangent (Figure 3(A)) is transformed to this 3D normal line. This transformation is a 3D normal-line transform in the cylinder, which is one of the main points of this paper. Note that Figure 4(A) shows a case where the P_t contact is at the O center of the visual field, but this transform holds for P_t with any position.

A curvature circle is detected as follows. As shown in Figure 4(B), performing this transformation for all tangents of the curvature circle (Figure 3(B)) causes these normal lines to intersect at one point $\mathbf{O_C}$, and thus the center (α_C,β_C) and radius r_C of the circle are detected as the coordinates of this intersection. Note that a 3D normal line outside each tangent is omitted for ease of viewing.

Therefore, the above first problem of not being able to detect the radius r has been resolved. In addition, the second problem is solved, as follows: each of the circles that make up a concentric circle can be detected separately, because this circle forms a different intersection at the corresponding height; thus, this problem has been solved.

2.2.2. Numerical verification of the curvature-circle detection

In order to verify that the curvature-circle detection (Figure 4(B)) can be correctly executed, each 3D normal line in the cylinder (α,β,r) was numerically calculated using equations (B3 to B5) of Appendix B, giving a curvature circle of radius r = 40 deg using eight tangents and contacts on its circumference. Then, a cross section of this cylinder was cut at each height r and arranged in Figure 5. In each cross section, intersections of these lines and the cross section were plotted.

Various behaviors that occur during this verification process (or occur at each cross section) will play an important role in the explanation of Figures 11, 12, 13, 14, and 15 and Section 5.2.2. Thus, these behaviors are described in detail below.

In (viii), the given eight contacts formed a circle with a radius of 40° which corresponded to the given circle, and this circle was shown in each cross section as dotted lines for reference: a normal line passing through each contact was shown as an alternate long and short dash line.

As the height r increased, this reference circle was divided into two circles composed of points, the inner circle became smaller, and the outer circle became larger. As shown in (v) as an example, the distance between the reference circle and this inner (or outer) circle is equal to the height coordinate r. This distance results from the V-shape representing the 3D normal line (Figure 4(A)): this is because increasing the height by r from the bottom causes the intersection of this V-shape with the cross section to move away (or shift) by r from the contact symmetrically. This shift from the contact along the normal line is a feature of this algorithm: note that the shift will be described later in detail in Section 5.2.2.

The inner circle decreased in size as r increased and then converged to one point at (iv). This convergence point corresponds to the intersection $\mathbf{O_C}$ of the 3D normal lines (Figure 4(B)). Thus, the center (α_C,β_C) and radius r_C of the curvature circle were detected as the coordinates of this convergence point. Therefore, the curvature-circle detection (Figure 4(B)) has been verified.

When the height r became higher than (iv), the inner circle was reversed and became larger again. On the other hand, the outer circle increased in size monotonically with height r.

2.2.3. Comparison with the detection on the plane

This circle detection on the eyeball is compared with that on the plane (Section 2.1). First, on the plane, the largest curvature circle is a straight line that represents a circle with an infinite radius, and thus this line can not be detected. On the other hand, on the eyeball, the largest curvature circle is a great circle whose radius is finite (i.e. π/2), and thus can be detected. Next, on the plane, curvature circles whose centers O_C protrude from the rectangular solid (x,y,r) can not be detected. On the other hand, on the eyeball, the center (α,β) of any curvature circle does not protrudes from the cylinder (α,β,r) and exists inside it, so any curvature circle can be detected. To summarize the above, this circle detection on the eyeball has the ability to detect arbitrary curvature circles, including the largest curvature circle (i.e. the great circle).

This ability allows to process an arbitrary figure in space composed of straight lines and curves using only circles on the eyeball. This is due to the following: (1) each straight line and curve in space can be transformed into a great circle and curve, respectively, when projected onto the eyeball; (2) these great circle and curve are a type of circle on the eyeball, because this curve is constituted by a group of curvature circles in contact with it; (3) therefore, this figure in space can be processed using only circles on the eyeball, when projected onto it.

3. Cell model

Figure 6 shows a series of cell models for detecting a curvature circle on the eyeball: the LGN cell, NDS simple cell, and CDC. The LGN and NDS simple cells were previously modeled, and reflect the response to various

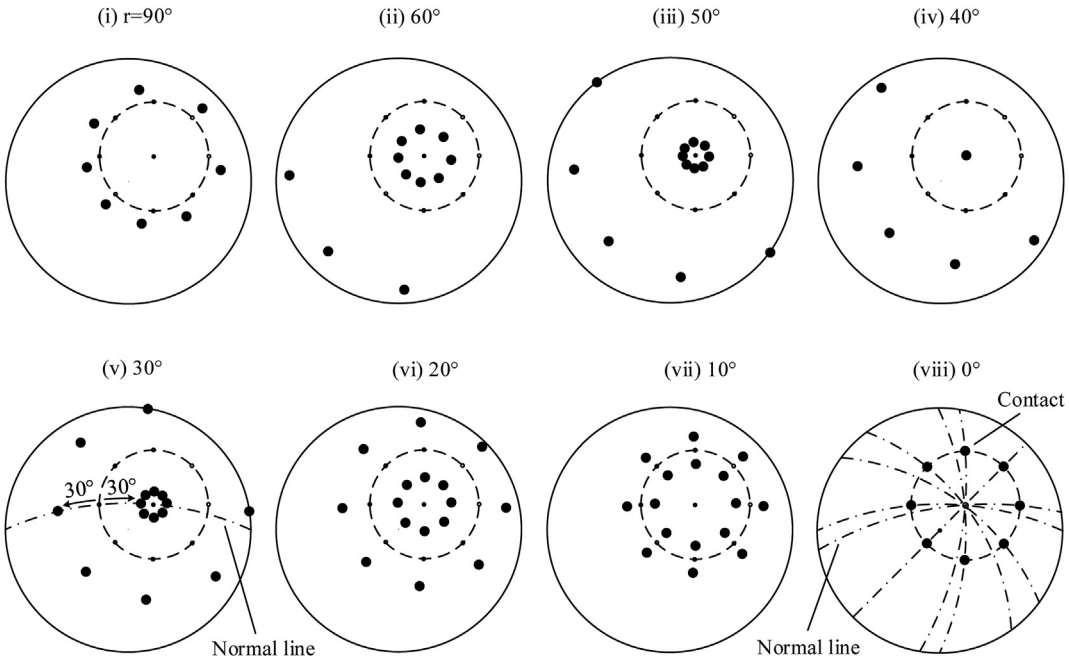

Figure 5. Numerical confirmation of the curvature-circle detection. In order to confirm that the curvature-circle detection in the cylinder (Figure 4(B)) is correctly performed, we calculated the 3D normal lines in it using equations (B3 to B5) in Appendix B. This cylinder was cut at each height r, and then its cross section was arranged in this figure. In each cross section, intersections of the 3D normal lines calculated above and this cross section were plotted. A curvature circle of radius r = 40 deg was given on the eyeball using eight contacts on its circumference. In (viii), the given eight contacts formed a circle with a radius of 40° which corresponds to the given circle, and a normal line passing through each contact was shown as an alternate long and short dash line. This formed circle was shown in each cross section as dotted lines for reference. As the height r increased, this reference circle was divided into two circles composed of points, the inner circle became smaller, and the outer circle became larger. As shown in (v) as an example, the distance between the reference circle and this inner (or outer) circle is equal to the height coordinate r. The inner circle decreased in size as r increased and then converged to one point at (iv). This indicates that the 3D normal lines intersected at this point, and thus the curvature circle was correctly detected as the coordinates of this point.

stimuli in actual LGN and NDS simple cells (Kawakami and Okamoto, 1996; Kawakami, 1996; Blasdel, 1992; Okamoto et al., 1999). The CDC will be modeled in Section 3.1 based on the algorithm in Section 2.2.

As a first explanation of Figure 6, the arrays of the retinal, LGN, and NDS simple cells and a pattern activated within each array are described, as follows. First, in (A), the eyeball surface is divided into local regions (i.e. receptive fields (RFs)), and the RFs superimposed on a curvature circle are shown. Next, the (B) shows a series of cell models for detecting each tangent of the circle. The (i) shows a circular array (x,y) composed of retinal cells in each RF, in which about 1000 cells exist and cells on this tangent are fired: dots (●) represent activated cells. The (ii) shows a circular array (x,y) of LGN cells, in which also about 1000 cells exist and the outline of the tangent in (i) is emphasized. This enhancement is done by a neural network performing the convolution between the retinal cell responses and the DOG filter: this convolution is hereinafter abbreviated as a DOG convolution. The (iii) shows a rectangular array (ρ,θ) of NDS simple cells, in which about 1000 cells are arranged. An NDS simple cell with the (ρ,θ) coordinates performs the Hough transformation of the LGN cell responses to detect the tangent in (ii), as follows. A network of Hough transform shown in (iii) causes this simple cell to be connected with all LGN cells on the tangent. By the network, this simple cell accumulates all LGN cell responses on the tangent and thus fires to detect the tangent corresponding to its coordinates (ρ,θ). Using this tangent detection, the CDC will be modeled below.

3.1. Basic CDC model

Figure 6(C) shows an arrangement of CDCs in the cylinder (Figure 4(A)), where this arrangement has been named a CDC column. Each cell in this column is expressed as CDC(α,β,r) that detects a curvature circle whose center and radius are (α,β) and r respectively.

A network that performs the 3D normal-line transform (Section 2.2.1)–that is, a network that connects each NDS simple cell ((B)(iii)) to all CDCs ((C)) on a 3D normal line within the CDC column–is modeled as follows: (1) the tangent in a LGN cell array ((B)(ii)) corresponding to each RF ((A)) is detected by an NDS simple cell ((B)(iii)) with the (ρ,θ) coordinates, as describe above; (2) then, this tangent is transformed to a 3D normal-line in the cylinder (Figure 4(A)), as described in Section 2.2.1; (3) since this cylinder corresponds to the CDC column, this tangent is transformed to a 3D normal-line in the column; (4) expressing the above with a network, this simple cell ((B)(iii)) detecting the tangent is connected to all CDCs ((C)) on the 3D normal line in the column. Thus, the network performing the 3D normal-line transform has been modeled as this connection.

A curvature circle is detected as follows. First, based on this network belonging to an RF ((A)), each NDS simple cell ((B)(iii)) in the (ρ,θ) array activates all CDCs ((C)) on the 3D normal line corresponding to this simple cell, thus generating a V-shaped pattern composed of activated CDCs in the column. Next, applying this network for all RFs superimposed on the curvature circle ((A)) causes a large number of these V-shaped patterns to occur in the column, as shown in Figure 4(B): patterns outside the contact were omitted for ease of viewing. Finally, a CDC at the intersection $\mathbf{O_C}$ of these patterns is fired most intensively, and thus the center (α_C,β_C) and radius r_C of the circle are detected as the coordinates of this intersection.

Thus, the CDC has been modeled by this network performing the 3D normal-line transform: in other words, the CDC has been modeled as the 3D normal-line transformation of NDS simple cell responses. This CDC can be also modeled as a convolution between the NDS simple cell responses and a synaptic weight matrix that represents this network.

This CDC detects every curvature circle constituting the contour of an arbitrary figure, and thus converts the contour composed of points into a set of the centers (α,β) and radii r of these circles (Section 2). In other

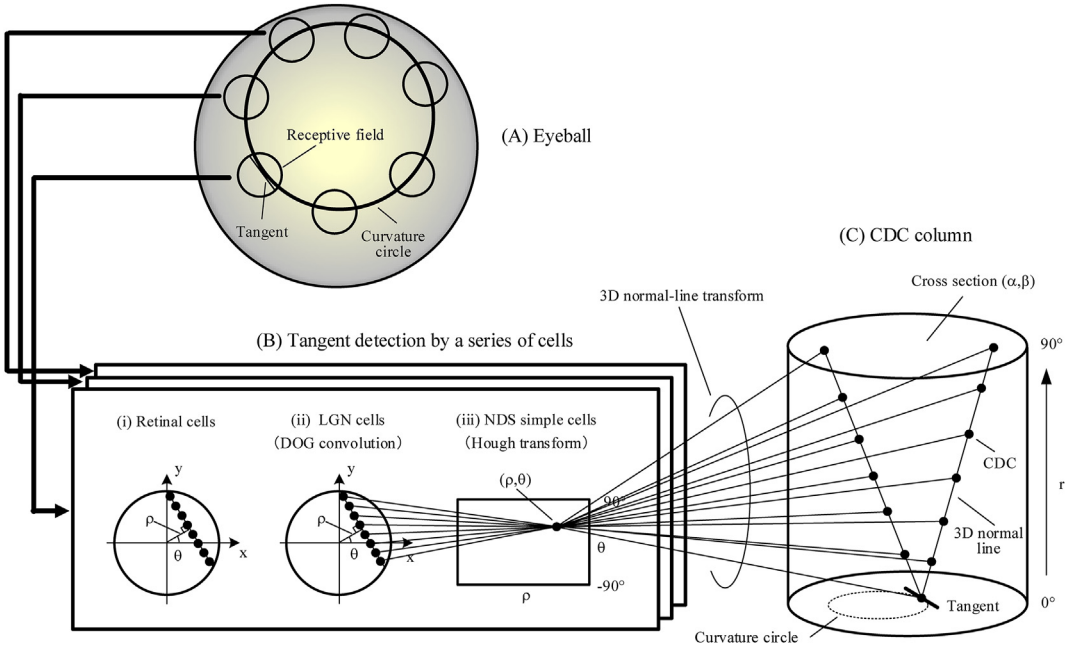

Figure 6. A series of modeled cells for detecting a curvature circle. This series is composed of LGN cells, NDS simple cells, and CDCs, which performs the DOG convolution, Hough transform, and 3D normal-line transform, respectively. The LGN and NDS simple cells were previously modeled (Kawakami and Okamoto, 1996; Kawakami, 1996; Okamoto et al., 1999). (A) The eyeball is divided into local regions (i.e. receptive fields (RFs)), and the RFs superimposed on a curvature circle are shown. (B) A series of cells for detecting each tangent in contact with the curvature circle is shown. The (i) shows a circular array (x,y) of retinal cells in each RF, in which about 1000 cells exist and cells on the tangent are fired. Dots (●) indicate activated cells. The (ii) shows a circular array (x,y) of LGN cells, in which also about 1000 cells exist and the outline of the tangent in (i) is emphasized by the DOG convolution. The (iii) shows a rectangular array (ρ,θ) of NDS simple cells, in which about 1000 cells are arranged. A simple cell with the (ρ,θ) coordinates performs the Hough transformation of the LGN cell responses to detect the tangent in (ii): this simple cell is connected to all LGN cells on the tangent, and this connection represents the network performing Hough transform. (C) An arrangement of CDCs in the cylinder (Figure 4(A)) is shown, and has been named a CDC column. Each cell in this column is expressed as CDC(α,β,r), which detects a curvature circle with the center (α,β) and radius r. The NDS simple cell at (ρ,θ) is connected to all CDCs on the corresponding 3D normal-line within the CDC column. This connection represents the network performing the 3D normal-line transform. This network causes each NDS simple cell to fire all CDCs on the corresponding 3D normal line.

words, the CDC allows the contour to be converted into a firing pattern, within the (α,β,r) CDC column, which is generated by detecting these circles. This CDC is, to our knowledge, the first cell model that detects the center and radius of this circle, including the modeling of the network performing the 3D normal-line transform.

Figure 6 is functionally composed of a series of transforms: the DOG convolution, Hough transform, and 3D normal-line transform. These transforms are performed by three types of operation: the addition, subtraction, and multiplication with constant coefficients. These operations are implemented by three types of synaptic function of neurons (Kuffler et al., 1984), respectively: the postsynaptic excitation, postsynaptic inhibition, and synaptic transmission efficiency. Thus, these three cell types have been modeled using the operations that can be implemented with neuron's synaptic functions.

We point out that equations (B3 to B5) in Appendix B representing the 3D normal lines are complicated, but there is no problem for the following reason. These equations are necessary to determine the network that connects each NDS simple cell to all CDCs on the 3D normal line, but once the network is determined, this equation is not necessary: in other words, the equations (B3 to B5) calculate the above network performing the 3D normal-line transform. Therefore, these complicated equations have no problem for CDC to work.

3.2. Cell arrangement in the CDC column

The CDCs in the column (Figure 6(C)) were assumed to be arranged at equal intervals, but it is not clear why it is so arranged. Therefore, let us determine the CDC arrangement based on the following two psychological considerations.

First, the large circle looks the same even if its size changes somewhat, whereas the small circle looks different even if its size changes a little. Assuming a discrimination threshold for the radius r of this circle (i.e. a minimum distinguishable radius threshold) to be Δr, this psychological consideration means that the larger the radius r, the larger Δr becomes. This relationship is expressed by the following equation as a first order approximation, where k_r is a constant coefficient to should be determined.

$$\Delta r = k_r\, r \tag{3}$$

Second, let us apply the same consideration to a center position (α,β) of circle. A large circle looks like the same position even if its center moves somewhat, whereas a small circle looks like a different position even if its center moves a little. Assuming a discrimination threshold for the position (α,β) of this circle (i.e. a minimum distinguishable position threshold) to be $\Delta_{\alpha\beta}$, this psychological consideration means that the larger the radius r, the larger $\Delta_{\alpha\beta}$ becomes. This relationship is expressed by the following equation as a first order approximation, where $k_{\alpha\beta}$ is a constant coefficient to should be determined.

$$\Delta_{\alpha\beta} = k_{\alpha\beta}\, r \tag{4}$$

This consideration on how the position of a circle with radius r looks signifies that one can detect every circle with radius r that exists in a ring whose radius and width are r and $\Delta_{\alpha\beta}$ respectively: this $\Delta_{\alpha\beta}$ increases with r due to this equation. Note that this signification is illustrated in Section C.1 of Appendix C using Figure C1(B).

Based on these considerations, we have determined the two intervals of the CDC arrangement in this column, as follow: (1) an interval of its height arrangement is equal to the discrimination threshold Δr that is expressed by Eq. (3): (2) an interval of the arrangement within each cross

section is equal to the threshold $\Delta_{\alpha\beta}$ that is expressed by Eq. (4). We point out that these equations have the same form as the Weber–Fechner law (Stanislas, 2003).

However, the neurophysiological basis for these equations is not clear. In order to address this issue, focusing on the discrimination $\Delta\theta_{SC}$ in θ orientation of an NDS simple cell, we derived the equation (C4) in Appendix C neurophysiologically. This equation (C4) is expressed as follows:

$$\Delta_{\alpha\beta} = (\Delta\theta_{SC}/2)\, r \tag{5}$$

The coefficient $k_{\alpha\beta}$ in Eq. (4) was also derived as $\Delta\theta_{SC}/2$, and the $\Delta\theta_{SC}$ is about 10° (Appendix B of Kawakami and Okamoto (1996) and Kawakami (1996)).

There is still one problem to solve, as follows. This Eq. (5) was derived for the curvature-circle detection on the plane, but the CDC detects the curvature circle on the eyeball. In order to address this issue, we derived in Appendix C the following equation suitable for the detection on the eyeball.

$$\Delta_{\alpha\beta} = (\Delta\theta_{SC}/2)\, \sin r \tag{6}$$

For Δr in Eq. (3), we assume that it is the same as the above $\Delta_{\alpha\beta}$, and thus the Δr is expressed as follows:

$$\Delta r = \Delta_{\alpha\beta} \tag{7}$$

Let us describe concretely how the CDCs are arranged in the column according to Eqs. (6) and (7). Since the interval Δr of the height arrangement was determined by Eq. (7), the larger r is, the coarser the CDC is arranged in the height direction. In addition, since the interval $\Delta_{\alpha\beta}$ within each cross section was determined by Eq. (6), the larger r is, the coarser the CDC is arranged within the cross section corresponding to the r. Thus, these equations cause the coarse-to-fine arrangement along the r-axis to be formed in the CDC column, including the arrangement within each cross section. This CDC arrangement is shown in Figure 7, where each dot (●) represents a CDC.

A small pink circle (Figure 7) centered on each CDC within a cross section of height r represents a range for dropout prevention, as follows. This CDC detects all curvature circles with the radius r whose centers are within this small circle. Therefore, this CDC, which detects these circles as a representative, can prevent these circles from dropping out. Next, we extend this small circle in the height direction to form a mini-column with a height Δr. A CDC at the center of this mini-column detects all curvature circles with the radius r whose centers are within this column, as their representative, and thus can prevent these circles from dropping out: note that this CDC, which should be in the center of the column, is drawn on its top for ease of viewing.

We point out that this discrimination threshold $\Delta_{\alpha\beta}$ (Eq. (6)) will play an important role in explaining the trade-off exhibited by actual cells in area V4 (see Section 5.1.3 described later).

3.3. CDC model based on the coarse-to-fine arrangement

Based on the above considerations, we have replaced the CDC column (Figure 6(C)) with the column in Figure 7 which has the coarse-to-fine arrangement. Similar to Figure 6, we connect each NDS simple cell (Figure 6(B)(iii)) to all CDCs on a 3D normal line in this replaced column. This connection represents a network that performs the 3D normal-line transform in this column. This network detects the curvature circle in the same way as described in section 3.1. Thus, the CDC based on this arrangement has been modeled.

This CDC column is constituted by discretely arranged CDCs (each of which exist at the center of a mini-column), but no dropout of curvature-circle detection occurs: this is because each CDC can detect all curvature circles whose center are within this mini-column (Section 3.2). Therefore, this discrete and coarse-to-fine arrangement greatly reduces the

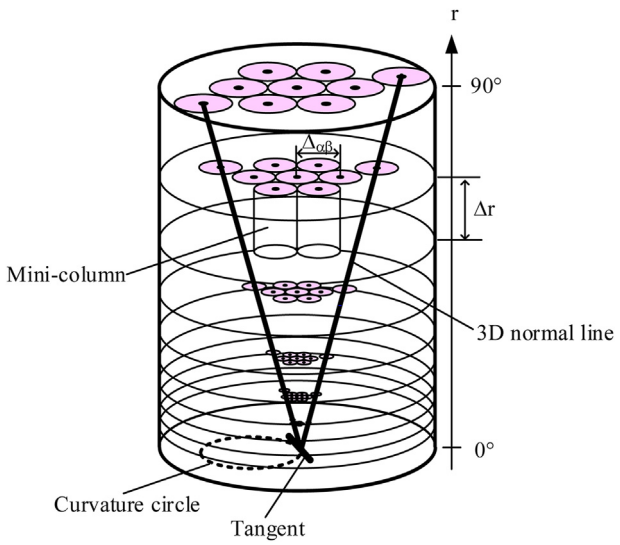

Figure 7. Cell arrangement in the CDC column. In the column of Figure 6(C), the CDCs were assumed to be arranged at equal intervals, but the basis of this arrangement is not clear. In order to address this issue, we have determine the intervals of this arrangement using Eqs. (6) and (7) that were derived based on neurophysiological considerations. This figure shows how the CDCs are arranged in the column according to these equations. Since the interval Δr of the height arrangement was determined by Eq. (7), the larger r is, the coarser the CDC is arranged in the height direction. In addition, since the interval $\Delta_{\alpha\beta}$ within each cross section of the column was determined by Eq. (6), the larger r is, the coarser the CDC is arranged within the cross section corresponding to the r. Thus, these equations cause the coarse-to-fine arrangement of CDC to be formed along the r-axis. Each mini-column represents a range for dropout prevention, as follows. Each dot (●) represents a CDC at the center of this mini-column: note that this dot, which should be drawn at the center of the column, is drawn on its top for ease of viewing. This CDC with the height r detects all curvature circles with the radius r whose centers are within this mini-column, as their representative, and thus can prevent the dropouts of these circles.

number of CDCs within the CDC column, because each mini-column has only one CDC in its center.

We point out that this CDC can detect not only the entire curvature circle but also a part of it (i.e. a circular arc) such as the local contour (Figure 1(A)): these detections will be later confirmed in Section 4.4.

3.4. Features of the CDC model

This CDC has three features. The first feature is its ability to process an arbitrary figure in space composed of straight lines and curves using only circles on the eyeball (Section 2.2.3). This feature results from the projection onto the eyeball. This is because any straight line in space is transformed to a great circle on the eyeball by this projection, and thus it can be processed as a kind of circle: an example of this ability will be shown later in the computer simulation (Figure 12).

The second feature is its ability for an arbitrary figure to be reconstructed by CDCs that detect all curvature circles constituting this figure. This reconstruction can be specifically described as follows. Each curvature circle is detected by a CDC. Then, a circle that corresponds to the center (α,β) and radius r of this detected circle is drawn on the eyeball, with its intensity equal to this CDC response. Performing this drawing for all detected circles causes the figure to be reconstructed as an envelope of these circles: an example of this reconstruction will be described later in the computer simulation (Figure 15(E)(iv); Section 4.4). We point out that this reconstruction resembles that based on the Fourier transform.

The third feature is its ability to sort and extract various components of the figure in the order of coarse-to-fine. This is due to the structure of the CDC column that has the coarse-to-fine arrangement along its r height axis (Figure 7). In a high cross section of the column, coarse components

composed of large curvature circles are extracted. In a low cross section, fine components composed of small curvature circles are extracted. Thus, the components included in this figure are sorted and extracted in the order of coarse-to-fine along the r axis: this extraction will be later confirmed by the description in Sections 4.3 and 4.4.

It is described below that these three features results from the (α,β,r) arrangement of the CDC column.

The first feature results from the (α,β) cross section of this arrangement. This is because this cross section corresponds to the eyeball (Section 2.2.1) onto which the figures in space are projected, as described above, and thus this projection produces this feature.

The reconstruction characterizing the second feature can be derived based on this (α,β,r) arrangement, as follows: (1) the 3D normal-line transform causes an arbitrary figure on the eyeball to be converted into a pattern of activated CDCs within this (α,β,r) arrangement (Section 3.1; Figure 6(C)); (2) then, draw a circle (on the eyeball) that corresponds to the (α,β,r) coordinates of each CDC in this pattern, with its intensity equal to this CDC response; (3) finally, performing this drawing for all CDCs in this pattern causes the figure to be reconstructed as an envelope of these circles; (4) thus, the reconstruction described above has been derived. This means that the essence of reconstruction lies in this (α,β,r) arrangement and the 3D normal-line transform generating this activated pattern. Therefore, the second feature has resulted from this (α,β,r) arrangement.

The third feature results from the r axis of this (α,β,r) arrangement, because the curvature circles constituting an arbitrary figure are extracted along this r axis in the order of coarse-to-fine as described above.

Based on these considerations, we think that this (α,β,r) arrangement of the CDCs, as well as the above abilities of the first and third features, plays an important role in shape recognition performed in area IT.

3.5. CDC model having perceptual constancy

In area IT at the end of the ventral pathway, cells having perceptual constancy were reported (Ito et al., 1995; Tanaka, 1996; Rust and DiCarlo, 2010; Zoccolan et al., 2007): these cells responded invariant to the translation or size change of a figure.

In area V4 that provides an information to area IT, two types of cell having perceptual constancy were reported: (1) the first type exhibits an invariance to the translation of a local contour of the figure, and is called a position-invariant cell (Pasupathy & Conner, 1999, 2001, 2002), which corresponds to the first cell type described in Section 1; (2) the second type exhibits an invariance to the size change (i.e. the curvature change) of the contour, and is called a size-invariant cell (i.e. a curvature-invariant cell) (El-Shamayleh and Pasupathy, 2016), which corresponds to the second cell type described in Section 1.

Based on these reports, in Sections 3.5.1 and 3.5.2, we will model two types of CDC having the constancy, which will be named constancy CDCs: (1) a position-invariant CDC that responds invariant to the center position (α,β) of a stimulus circle; (2) a curvature-invariant (i.e. size-invariant) CDC that responds invariant to its radius r (i.e. to its size). Then, these constancy CDCs will be shown to correspond to the above two types of area V4 cell, respectively.

Prior to modeling, the selectivity of the cell CDC(α_0,β_0,r_0), which is the basis for these constancy CDCs, is shown in Figure 8(A): the ordinate represents the CDC response to a stimulus circle whose center and radius are (α,β) and r, respectively, where the disk (α,β) is the equidistant projection of the eyeball surface (Figure 4(C)(ii)); the subscript "0" indicates that the CDC responds selectively to the parameter having this subscript (e.g. (α_0,β_0)). This CDC selectively responds to both center (α_0,β_0) and radius r_0 of the stimulus circle: in other words, the cell CDC(α_0,β_0,r_0) detects both center (α_0,β_0) and radius r_0 of the circle. The widths $\Delta_{\alpha\beta}$ and Δ_r of these selective responses are expressed by Eqs. (6) and (7), and correspond to the diameter and height of the mini-column (Figure 7), respectively.

3.5.1. Position-invariant CDC

This CDC denoted as $CDC_{\alpha,\beta}(r_0)$ is modeled as an operation composed of two successive steps, as follows: in the first step, the positive component of a cell response CDC(α,β,r_0) is output, then in the second step this output is accumulated over its (α,β) center coordinates within the RF, and thus the cell response $CDC_{\alpha,\beta}(r_0)$ is obtained. This operation has been named a positive-component accumulation. This response $CDC_{\alpha,\beta}(r_0)$ is expressed as the following equation:

$$CDC_{\alpha,\beta}(r_0) = \Sigma_\alpha \Sigma_\beta \text{ Positive}(CDC(\alpha,\beta,r_0)) \quad (8)$$

The Σ and the Positive( ) represent an accumulation and a positive-component output, respectively. This positive-component accumulation is a type of pooling, and corresponds to the max-pooling of Cadieu et al. (2007).

Thus, this cell $CDC_{\alpha,\beta}(r_0)$ has been modeled as the positive-component accumulation of the cell responses CDC(α,β,r_0) with the same r_0 radius selectivity but different (α,β) center selectivity, and the cell response is expressed by Eq. (8). This equation represents a network that connects each cell $CDC_{\alpha,\beta}(r_0)$ to all cells CDC(α,β,r_0) having the same r_0 radius selectivity.

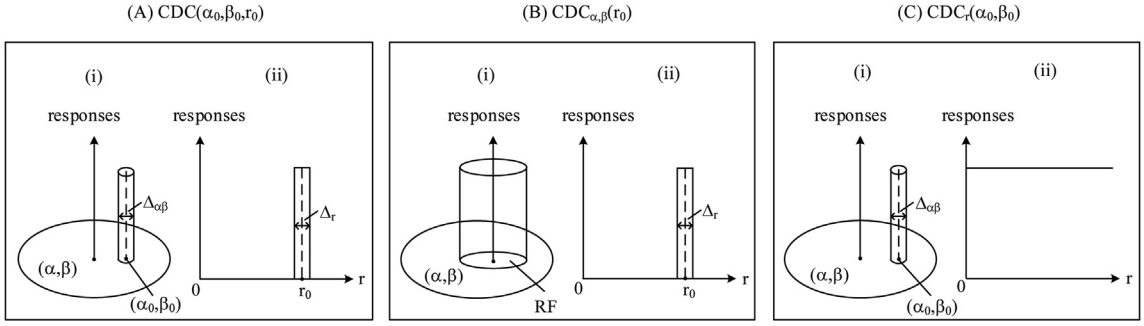

Figure 8. Response selectivities of three types of CDC. The ordinate represents the cell response to a stimulus circle, and the disk (α,β) represents the equidistant projection of the eyeball surface (Figure 4(C)(ii)). The (A) shows the selective response of a cell CDC(α_0,β_0,r_0), which is the CDC and was modeled in Section 3.1, to this circle. This cell responds selectively to a center (α_0,β_0) of the circle as shown in (i), and responds selectively to its radius r_0 as shown in (ii). In other words, it responds selectively to both center (α_0,β_0) and radius r_0 of the circle. The widths $\Delta_{\alpha\beta}$ and Δ_r of these responses are expressed by Eqs. (6) and (7), respectively. These widths are small, less than 5°, but are drawn large for ease of viewing: note that the RF in (B)(ii) is also drawn large for the same reason. The (B) shows the selective response of a cell $CDC_{\alpha,\beta}(r_0)$, which was modeled by Eq. (8), to the circle. This cell responds invariant to a center (α,β) of the circle within the RF as shown in (i), but selectively responds to its radius r_0 as shown in (ii). The (C) shows the selective response of a cell $CDC_r(\alpha_0,\beta_0)$, which was modeled by Eq. (9), to the circle. This cell responds invariant to a radius r of the circle as shown in (ii), but selectively responds to its center (α_0,β_0) as shown in (i).

Let us compare this cell $CDC_{\alpha,\beta}(r_0)$ with the above position-invariant cell in area V4. The cell $CDC_{\alpha,\beta}(r_0)$ responds invariant to a center (α,β) of a stimulus circle within an RF, but selectively responds to its radius r_0 (Figure 8(B)). On the other hand, the position-invariant cell in area V4 responds invariant to the translation of the circle, but selectively responds to its radius r_0 (Figure 9(A)). Since their invariance and selectivity are the same, the position-invariant CDC denoted as $CDC_{\alpha,\beta}(r_0)$ corresponds to this position-invariant cell.

This cell $CDC_{\alpha,\beta}(r_0)$ can detect every curvature circle with a radius r_0 whose center is within RF.

We note that this positive-component output was also used in the 3D normal-line transform (Section 3.1): specifically, a positive-component of each NDS simple cell (Figure 6(B)(iii)) was output to all CDCs on the 3D normal line (Figure 6(C)).

3.5.2. Curvature-invariant CDC

This CDC denoted as $CDC_r(\alpha_0,\beta_0)$ has been modeled as the positive-component accumulation of the cell responses $CDC(\alpha_0,\beta_0,r)$ with the same (α_0,β_0) center selectivity but different r radius selectivity. This cell response $CDC_r(\alpha_0,\beta_0)$ is expressed by the following equation.

$$CDC_r(\alpha_0,\beta_0) = \Sigma_r \text{ Positive}(CDC(\alpha_0,\beta_0,r)) \quad (9)$$

This equation represents a network that connects each cell $CDC_r(\alpha_0,\beta_0)$ to all cells $CDC(\alpha_0,\beta_0,r)$ having the same (α_0,β_0) center selectivity.

Let us compare this cell $CDC_r(\alpha_0,\beta_0)$ with the above curvature-invariant cell in area V4. The cell $CDC_r(\alpha_0,\beta_0)$ responds invariant to a radius r of a stimulus circle, but selectively responds to its center (α_0,β_0) (Figure 8(C)). On the other hand, the curvature-invariant cell in area V4 responds invariant to a scaling of the circle (i.e. to its radius r), but selectively responds to its center (α_0,β_0) (Figure 9(B)). Since their invariance and selectivity are the same, the curvature-invariant CDC denoted as $CDC_r(\alpha_0,\beta_0)$ corresponds to this curvature-invariant cell.

This cell $CDC_r(\alpha_0,\beta_0)$ can detect every curvature circle with a center (α_0,β_0), independently of its radius r, and thus responds intensively to a concentric circle, whose center is (α_0,β_0), to detect it. This response is proportional to the number of circles constituting the concentric circle.

3.6. Cell hierarchy from LGN cell to constancy CDCs

Integrating these two types of constancy CDC with the series of cells in Figure 6, we propose a cell hierarchy (Figure 10) that detects each curvature circle constituting an arbitrary figure. These three types of CDC possess the three features described in Section 3.4: the cell $CDC(\alpha,\beta,r)$ possesses the 1st to 3rd features, the cell $CDC_{\alpha,\beta}(r)$ possesses the 1st and 3rd features, and the cell $CDC_r(\alpha,\beta)$ possesses the 1st feature. These CDC types can detect not only the entire circle but also the local contour (i.e. a part of the circle).

This hierarchy is composed of the cells LGN(x,y), $SC_{NDS}(\rho,\theta)$, $CDC(\alpha,\beta,r)$, $CDC_{\alpha,\beta}(r)$, and $CDC_r(\alpha,\beta)$: these cells also represent their arrays or their responses. The hierarchy is functionally composed of a series of mathematical transforms: the DOG convolution, Hough transform, 3D normal-line transform, and two types of positive-component accumulation. Each transform represents a network that connects the front and back adjacent cell arrays, and is performed by the operations of the addition, subtraction, and multiplication with constant coefficients (Section 3.1). The operations can be implemented with synaptic functions of neurons (Section 3.1). Thus, this hierarchy has been modeled using the operations that can be implemented with neuron's synaptic functions.

The series of cells constituting this hierarchy, to our knowledge, has been systematically modeled in the neurophysiological processes for the first time, including the modeling of their networks performing these transforms.

This hierarchy has the following interesting properties (see Section 5.4 described later for details): (1) the hierarchy performs a series of conversions of cell array, specifically, each cell array is converted in the order (x,y), (ρ,θ), (α,β,r), and r (or (α,β)); (2) each cell-array conversion either creates new array parameters (i.e. new features) to acquire more complex feature or annihilates an array parameter to acquire the invariance to that parameter.

We point out the followings. First, each transform in the hierarchy represents a network that connects the adjacent cell arrays. For example, Hough transform represents a network (Figure 6(B)(iii)) that connects an NDS simple cell at (ρ,θ) to all LGN cells on the tangent. Second, this network is represented by a sparse matrix with respect to synaptic weights, except for the DOG convolution. For example, the above network of Hough transform is represented by a sparse matrix whose weights are determined by this transform: specifically, these weights have the value 1 in the matrix elements that satisfy the relationship $\rho - x\cos\theta - y\sin\theta = 0$ in a four-dimensional (4D) space (x,y,ρ,θ), and the value 0 in all other elements; thus, the weights form the sparse matrix that corresponds to a hyperplane within this 4D space (see Appendix D of Kawakami (1996)).

4. Simulation results

Computer simulations in Figures 11, 12, 13, 14, and 15 confirmed that the cells $CDC(\alpha,\beta,r)$ correctly detected curvature circles included in various stimuli, where the CDC column in Figure 6(C) was replaced with

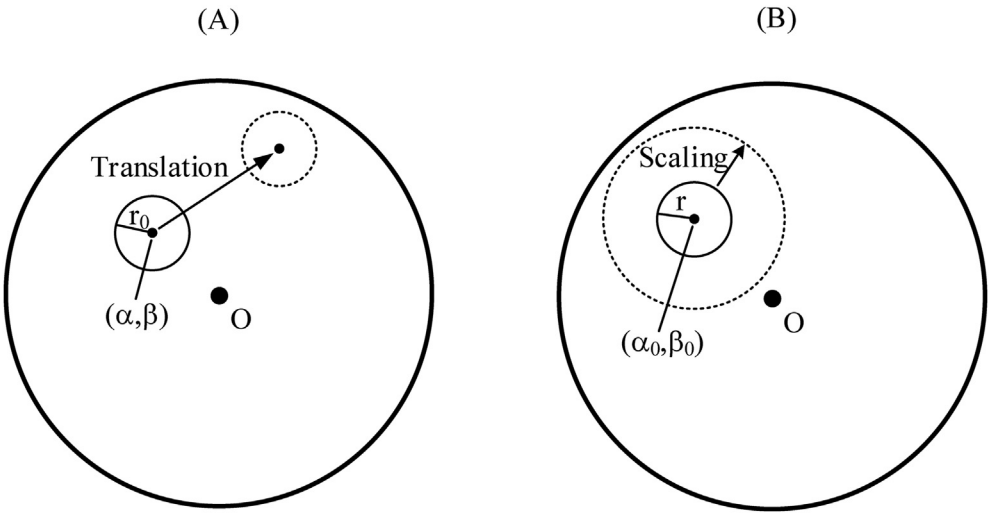

Figure 9. Two types of constancy cell in area V4. The disk shows the equidistant projection of the eyeball surface (Figure 4(C)(ii)), where O corresponds to the center of the visual field. The (A) shows the invariance of a position-invariant cell in area V4 to a center (α,β) of stimulus circle: specifically, even if this circle with radius r_0 translates on the eyeball, this cell response to it does not change. In other words, this cell responds invariant to the circle's center (α,β), but selectively responds to its radius r_0. The (B) shows the invariance of a curvature-invariant (i.e. a size-invariant) cell in area V4 to a radius r of stimulus circle: specifically, even if this circle with center (α_0,β_0) is scaled up, this cell response to it does not change. In other words, this cell responds invariant to the circle's radius r, but selectively responds to its center (α_0,β_0).

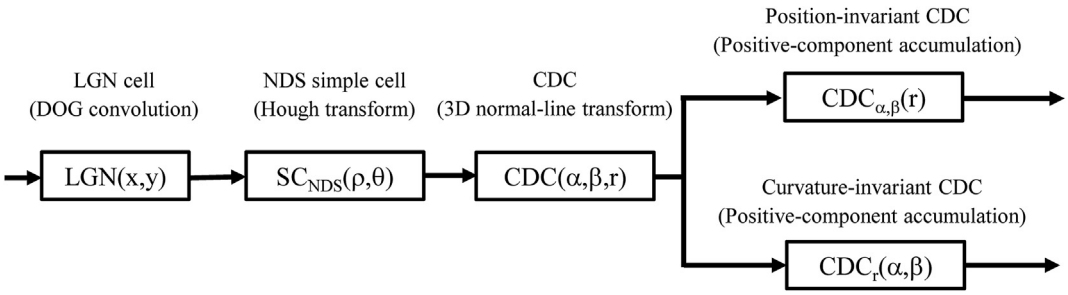

Figure 10. A hierarchy from LGN cell to two types of constancy CDC (i.e. the position-invariant and curvature-invariant CDCs). This hierarchy that detects curvature circles was obtained by integrating the series of cells (Figure 6) with the two types of constancy CDC (Section 3.5). It is composed of the cells LGN(x,y), $SC_{NDS}(\rho,\theta)$, CDC(α,β,r), $CDC_{\alpha,\beta}(r)$, and $CDC_r(\alpha,\beta)$. These cells perform the DOG convolution, Hough transform, 3D normal-line transform, positive-component accumulation (i.e. a type of pooling) of the cell responses CDC(α,β,r) preferring the same r radius, and that preferring the same (α,β) center, respectively.

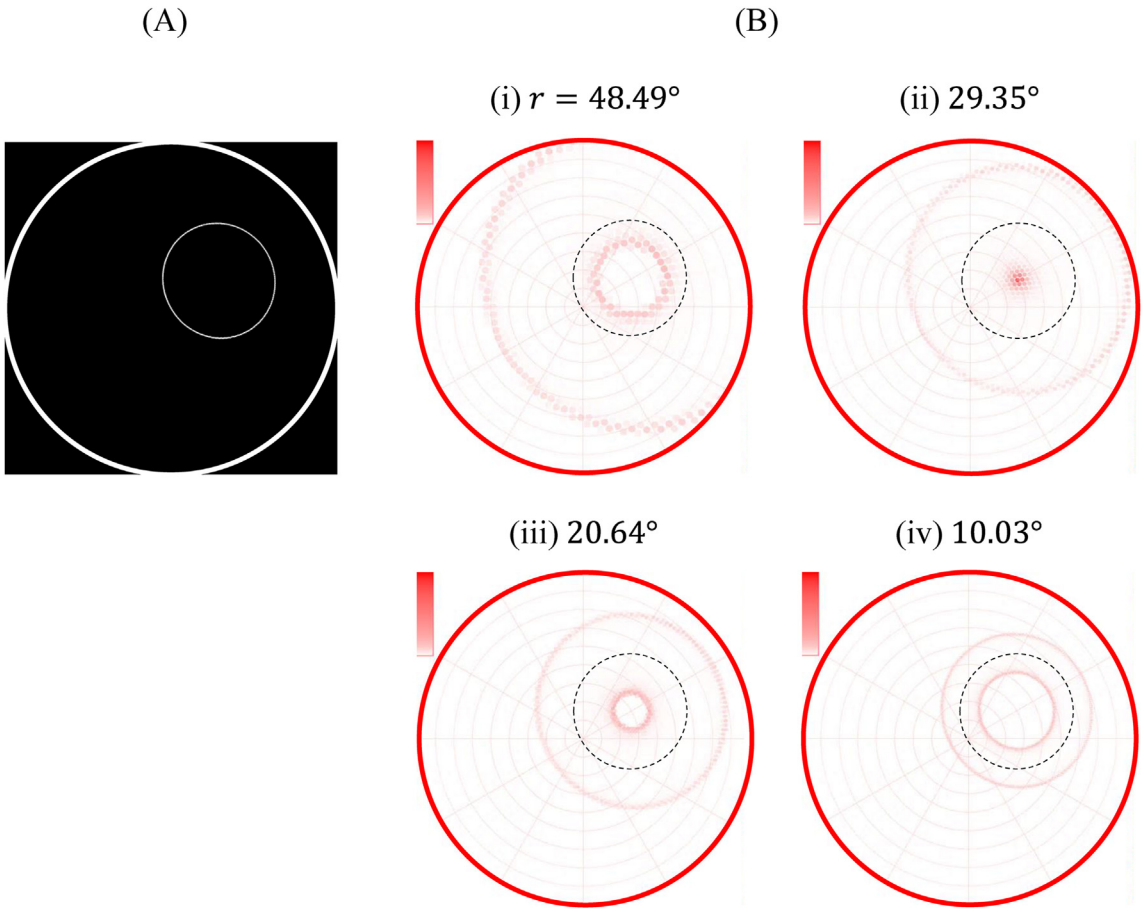

Figure 11. Responses of the CDCs to a circle. A circle on the eyeball was correctly detected by the corresponding CDC. (A) A circle, whose radius r and center (α,β) are 30° and (30°, 30°) respectively, was presented on the eyeball as a stimulus and is shown as the equidistant projection of it (Figure 4(C)). (B) The CDC column (Figure 6(C)) to this circle was cut at each height r, and its cross section was arranged: each dot (●) in every cross section represents the response of a CDC, the size of which is equal to a cross section of the mini-column (Figure 7); the latitude and longitude of the eyeball are also drawn; the scale bar (left) shows that the CDC response ranged from 0 (light red) to 255 (dark red). On each cross section, the presented circle was drawn as black dotted lines for reference. As the height r increased, this reference circle was divided into two circles, the inner circle became smaller, and the outer circle became larger: the distance between the reference circle and these circles was equal to the height coordinate r (Section 2.2.2). The radius of this inner circle became zero in (ii) and it converged to one point. This convergence point coincided with the center of the presented circle, and thus the circle was correctly detected as the coordinates of this point.

that in Figure 7 having the coarse-to-fine arrangement. The parameters used in these simulations are shown as follows: (1) those used in the simulation of Figure 6(B) were shown in Appendix B of Kawakami and Okamoto (1996); (2) those used in the simulation of Figure 6(C) were described in Section 3.3.

Brief overviews are provided below to highlight the content of the following subsections.

In Section 4.1, we will present a circle to the eyeball to show that the series of modeled cells in Figure 6 can detect the circle correctly.

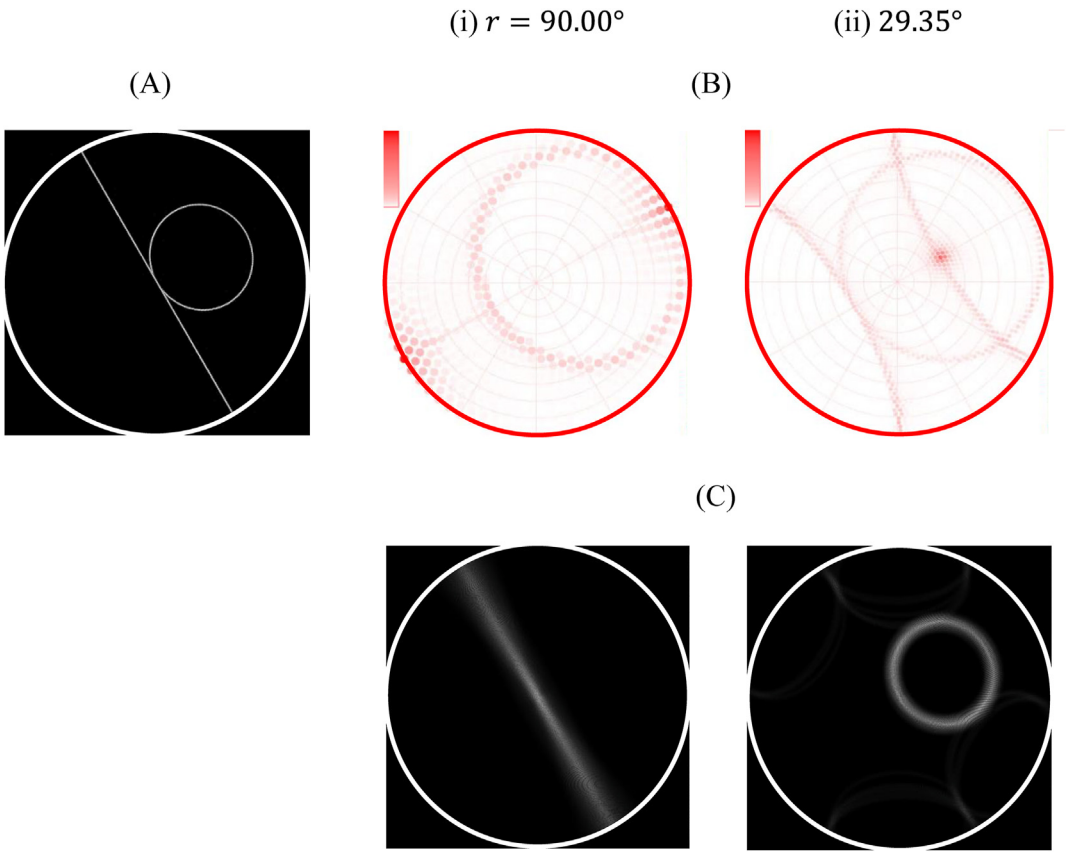

Figure 12. Responses of the CDCs to a great and small circles. These circles on the eyeball, which correspond to a straight line and circle in space respectively, were correctly detected by the corresponding CDCs. (A) These circles were presented on the eyeball (Figure 6(A)), which are shown as the equidistant projection of them. The radius r and center (α,β) of the great circle are respectively 90° and (30°, 90°), and those of the small circle are respectively 30° and (30°, 30°). (B) Two cross sections of the CDC column are shown. In (i), a CDC whose center (α,β) and radius r are (30 deg, 90 deg) and 90° was maximally fired, and thus the presented great circle was correctly detected as the coordinates of this CDC. (Note the following: another CDC whose center exists the opposite position (i.e. (α = 30 + 180 deg, β = 90 deg)) fired with the same intensity; this is singular to a great circle passing through the center of the visual field, because the center of this great circle belongs to both (α = 30 deg, β = 90 deg) and (α = 30 + 180 deg, β = 90 deg)). In (ii), a cell whose center (α,β) is (30°, 30°) was maximally fired, and thus the center of the presented small circle was correctly detected as the coordinates of this CDC. On the other hand, there are two types of weakly firing patterns. These types can be explained by the description on the numerical confirmation (Section 2.2.2), as follows. The first type is a weakly circular-firing pattern in (ii) whose radius and center were 60° and (30°, 30°), respectively. This pattern corresponds to the outer circle composed of points in Figure 5(iv) that occurred at the moment when the inner circle converged to one point. The second type is a weakly circular-firing pattern in (i) whose radius and center are 60° and (30°, 30°), respectively. This pattern corresponds to the inner circle composed of points in Figure 5(i) that grew again after the above inner circle converged to one point. The same applies to two circles of (ii) passing through (α = 30 deg, β = 30 deg) and (α = 30 + 180 deg, β = 30 deg). (C) The eyeball images calculated reversely from the cross-sectional response of (B) using the network (Figure 6) are shown (Section 4.2). These reverse-calculated images match with the presented images on the eyeball (A).

In Section 4.2, we will present a great and small circles to the eyeball to show that the corresponding CDCs can detect them correctly. Since these great and small circles are the projection of a straight line and circle in space onto the eyeball (Section 2.2.3), respectively, this detection allows the first feature in Section 3.4 to be confirmed: this feature is the ability to process an arbitrary figure in space composed of straight lines and curves using only circles on the eyeball.

In addition, we will describe a reverse calculation method for calculating eyeball images reversely from the cross-sectional responses of the CDC column using the network (Figure 6). This method makes it possible to understand what kind of curvature circle each cross-sectional response of CDC detects, and plays an important role in evaluation of the curvature detection.

In Section 4.3, we will present a triangle to the eyeball, and will show that three types of curvature circles included in it (i.e. the great circles corresponding to its sides, the circle inscribed in the triangle, and the circles inscribed in the two sides) can be correctly detected at the corresponding heights of the CDC column (Figure 6(C)). This detection allows the third feature in Section 3.4 to be confirmed: this feature is the ability to sort and extract various components of a figure in the order of coarse-to-fine along the height axis of the column.

In Section 4.4, we will present a figure composed of various curvature circles to the eyeball, and will show that all curvature circles constituting this figure can be detected separately along the height axis of the column. These two types of detection allow the second and third features in Section 3.4 to be confirmed, respectively. First, the detection along the height axis allows the third feature to be confirmed as above. Second, the detection of all curvature circles constituting it allows the second feature to be confirmed: this second feature is the ability for an arbitrary figure to be reconstructed by CDCs that detect all curvature circles constituting this figure.

4.1. Circle

The simulation in Figure 11 confirmed that a circle on the eyeball was correctly detected by the corresponding CDC.

The (A) shows the equidistant projection of the eyeball surface, on which a circle whose radius r and center (α,β) are 30° and (30°, 30°)

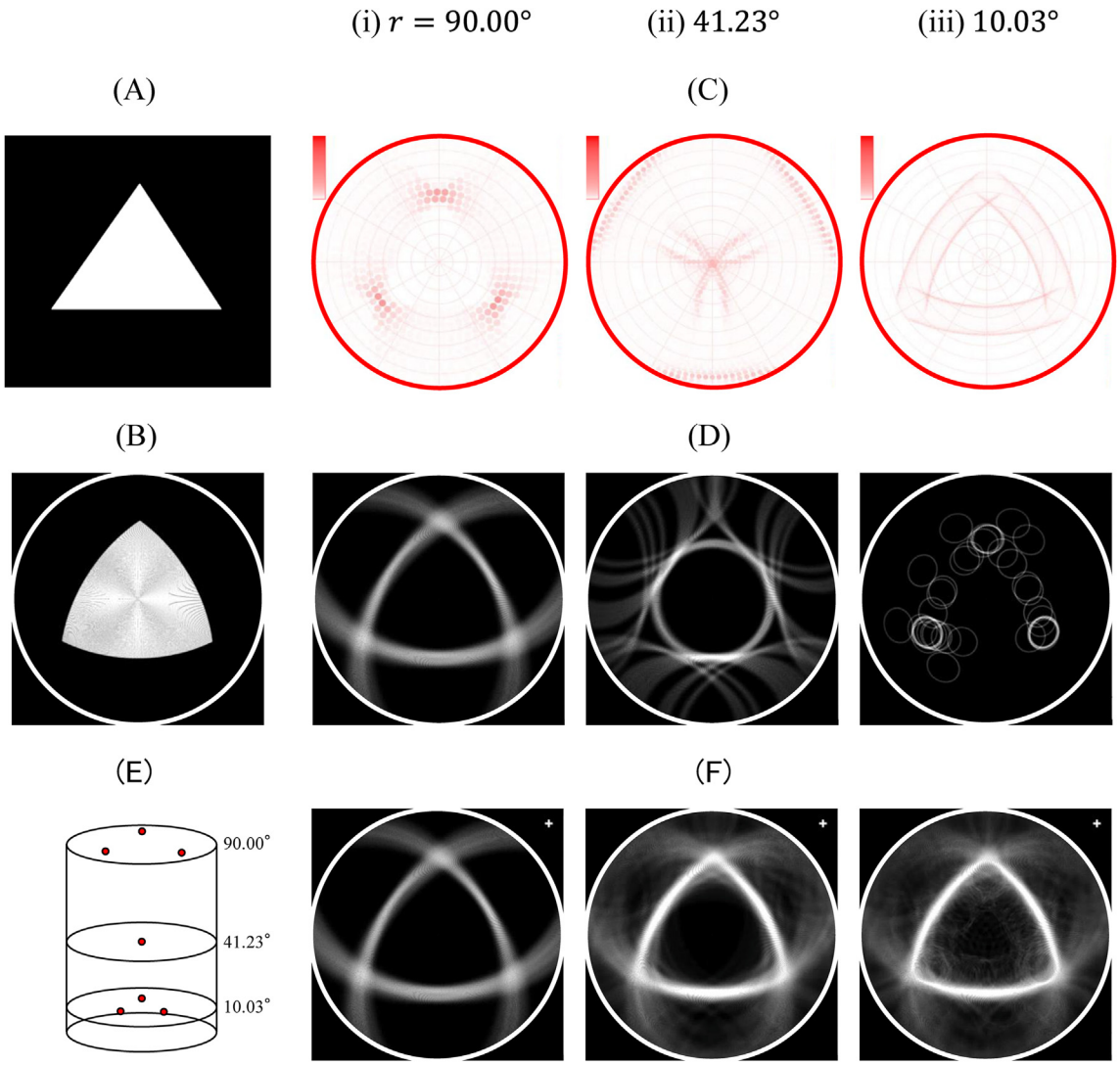

Figure 13. Responses of the CDCs to a triangle. Each curvature circle included in a triangle was correctly detected by a CDC whose height coordinate is equal to the circle's radius. (A) A triangle is shown on the plane. (B) It was projected onto the eyeball, and then was presented as a stimulus. (C) Cross-sectional responses of the CDC column to the triangle of (B) are shown. Three types of curvature circle included in the triangle (i.e. the great circles, the circle inscribed in the triangle, and the circles inscribed in the two sides) were respectively detected separately on heights r = 90, 41.23, and 10.03 deg corresponding to their radii. The double triangle in (iii) corresponds to the double circle composed of points (Figure 5(vii); Section 2.2.2): note that the double figure (Figures 14(C)(iii) and 15(C)(iv) shown later) also corresponds to this double circle. (D) The eyeball images calculated reversely from the cross-sectional responses of (C) using the network (Figure 6) are shown. The three types of curvature circle above were reverse-calculated as the great circles in (i), a circle inscribed in the three sides in (ii), and the circles inscribed in the two sides in (iii), respectively. (E) The center of each three circle type is schematically shown. (F) Each image was obtained by accumulating the reverse-calculated images of (D) in the order (i), (ii), and (iii). This accumulation progressed as the height r became smaller, and finally, in (iii), the presented triangle (B) was reconstructed.

respectively was presented as a stimulus. This circle caused CDCs within the column (Figure 6(C)) to be fired as shown in Figure 4(B). This column was cut at each height r and its cross section was arranged in (B). For reference, the presented circle was shown as black dotted lines on each cross section.

As the height r increased, the reference circle was divided into two circular activated patterns, the inner pattern became smaller, and the outer pattern became larger: this behavior is the same as in Figure 5, and can be explained by the description in Section 2.2.2. The radius of this inner pattern became zero in (ii) and it converged to one point. This convergence point coincided with the center of the presented circle.

There is an issue for the detection of radius r, that is, the cross section corresponding to the presented radius r = 30 deg did not exist in (B): this is because the r height axis of the column is arranged discretely (Section 3.3). However, the mini-column in Figure 7 could solve this issue and allowed the circle with r = 30 deg to be correctly detected by a CDC with r = 29.35 deg: this is because the CDC at the center of this mini-column (i.e. the CDC with r = 29.35 deg) could detect all curvature circles whose centers are within this column containing r = 30 deg.

Therefore, this simulation confirmed that the presented circle was correctly detected by the CDC whose radius and center are 29.35° and (α = 30 deg, β = 30 deg) respectively.

When height r exceeded 29.35 deg, this inner pattern was reversed and its size increased. On the other hand, the outer pattern monotonously increased in size with r. Why these behaviors occurred was described in section 2.2.2.

Finally, the responses of the cells $CDC_{\alpha,\beta}(r)$ and $CDC_r(\alpha,\beta)$ to this stimulus circle were confirmed, as follows. First, a cell $CDC_{\alpha,\beta}(r)$ whose r coordinate is 29.35° maximally responded to this circle, independently of its circle's center (α,β). These maximal and independent responses are the same as those shown in Figure 8(B)(ii) and Figure 8(B)(i), respectively. Thus, the responses characteristic of this cell $CDC_{\alpha,\beta}(r)$ were confirmed. Second, a cell $CDC_r(\alpha,\beta)$ whose (α,β) coordinates are (30°, 30°) maximally responded to this circle, independently of the circle's radius r.

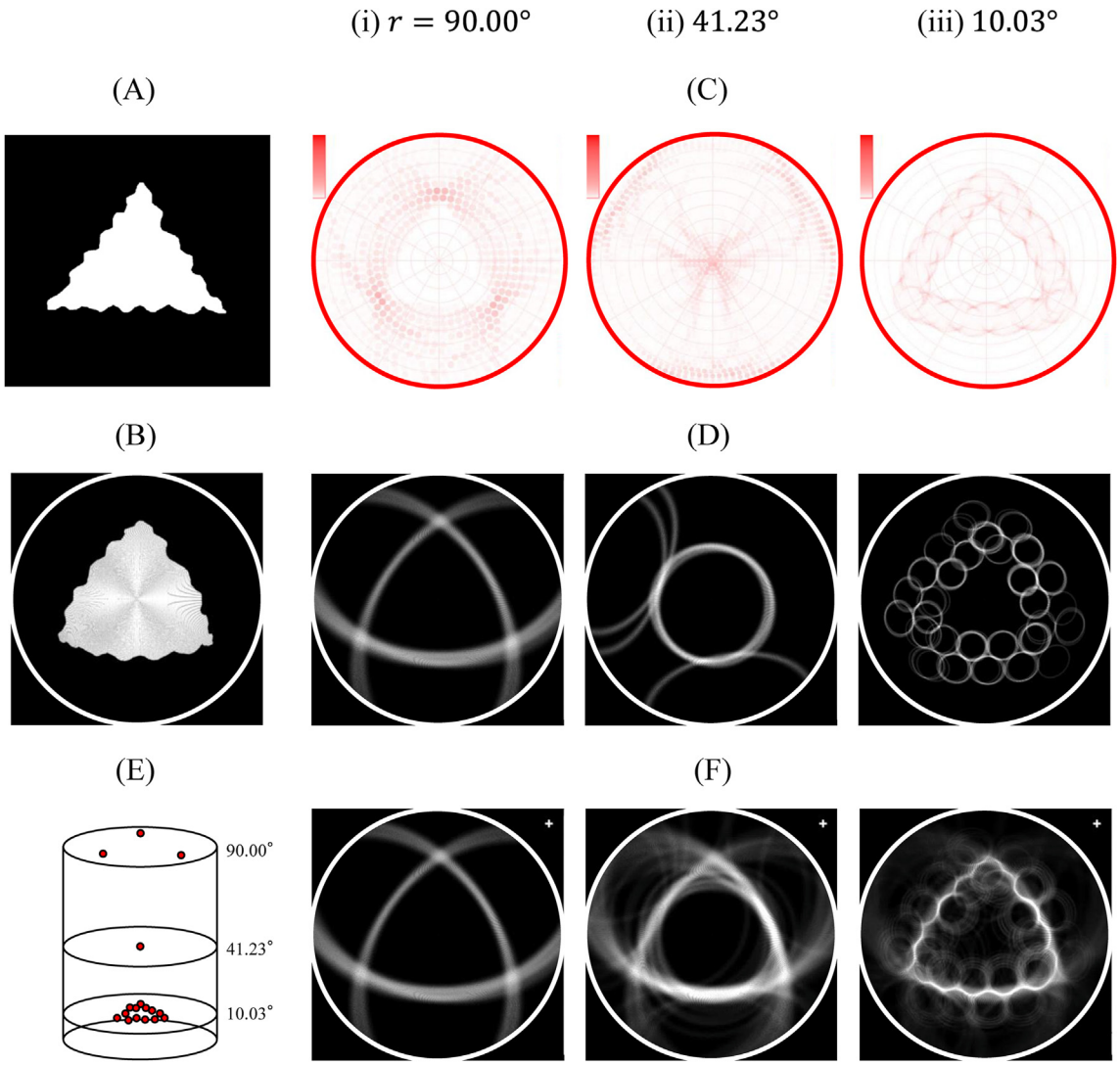

Figure 14. Responses of CDCs to a triangle with fine unevennesses. (A) A triangle obtained by adding fine unevenness to each side of the triangle (Figure 13(A)) is shown on the plane. (B) It was projected onto the eyeball, and then was presented as a stimulus. (C) Cross-sectional responses of the CDC column to the triangle of (B) are shown. (D) The eyeball images calculated reversely from the cross-sectional responses of (C) using the network (Figure 6) are shown. (E) The center of each three circle type is schematically shown. (F) Each image was obtained by accumulating the reverse-calculated images of (D) in the order (i), (ii), and (iii). This accumulation progressed as the height r became smaller, and finally, in (iii), the presented triangle (B) was reconstructed.

These maximal and independent responses are the same as those shown in Figure 8(C)(i) and (C)(ii), respectively. Thus, the responses characteristic of the cell $CDC_r(\alpha,\beta)$ were confirmed.

The computer simulations of these constancy CDCs were not shown. The reason is as follows. In order for the above evaluation of the maximal and independent responses, only the position of maximum response and the independence of response are necessary respectively, and these position and independence have been described above. Thus, the simulations were not shown.

4.2. Figure containing a great circle

The simulation in Figure 12 confirmed the first feature (Section 3.4) using a great and small circles on the eyeball, which are the projection of a straight line and circle in space onto the eyeball, respectively (Section 2.2.3).

The (A) shows the equidistant projection of the eyeball surface, on which a small and great circles were presented as stimuli. These circles caused CDCs within the column (Figure 6(C)) to be fired as shown in Figure 4(B). This column was cut at each height r and its cross section was arranged in (B). In (i), the cell at the position of ($\alpha = 30$ deg, $\beta = 90$ deg) fired maximally to detect the radius and center of the presented great circle. Also, in (ii), the cell at the position of ($\alpha = 30$ deg,$\beta = 30$ deg) fired maximally to detect the center of the presented small circle. The lack of the cross section of $r = 30$ deg is the same reason as described in section 4.1, and thus the presented circle was detected by this CDC with $r = 29.35$ deg.

Therefore, these great and small circles, which correspond to the straight line and curve in space respectively, were correctly detected. Thus, this detection have allowed the first feature above to be confirmed.

The (C) shows eyeball images that were calculated reversely from the cross-sectional responses of (B) using the network (Figure 6). The image of (C)(i) calculated from (B)(i) matches the great circle in (A), and the image of (C)(ii) calculated from (B)(ii) matches the small circle in (A). In this way, this reverse calculation makes it possible to understand what kind of curvature circle each cross-sectional response ((B)) detects, and plays an important role in evaluation of the curvature detection.

This calculation was performed, as follow. First, the image (C)(ii) calculated reversely from the response (B)(ii) is described. From every CDC activated in (B)(ii), the network of the 3D normal-line transform

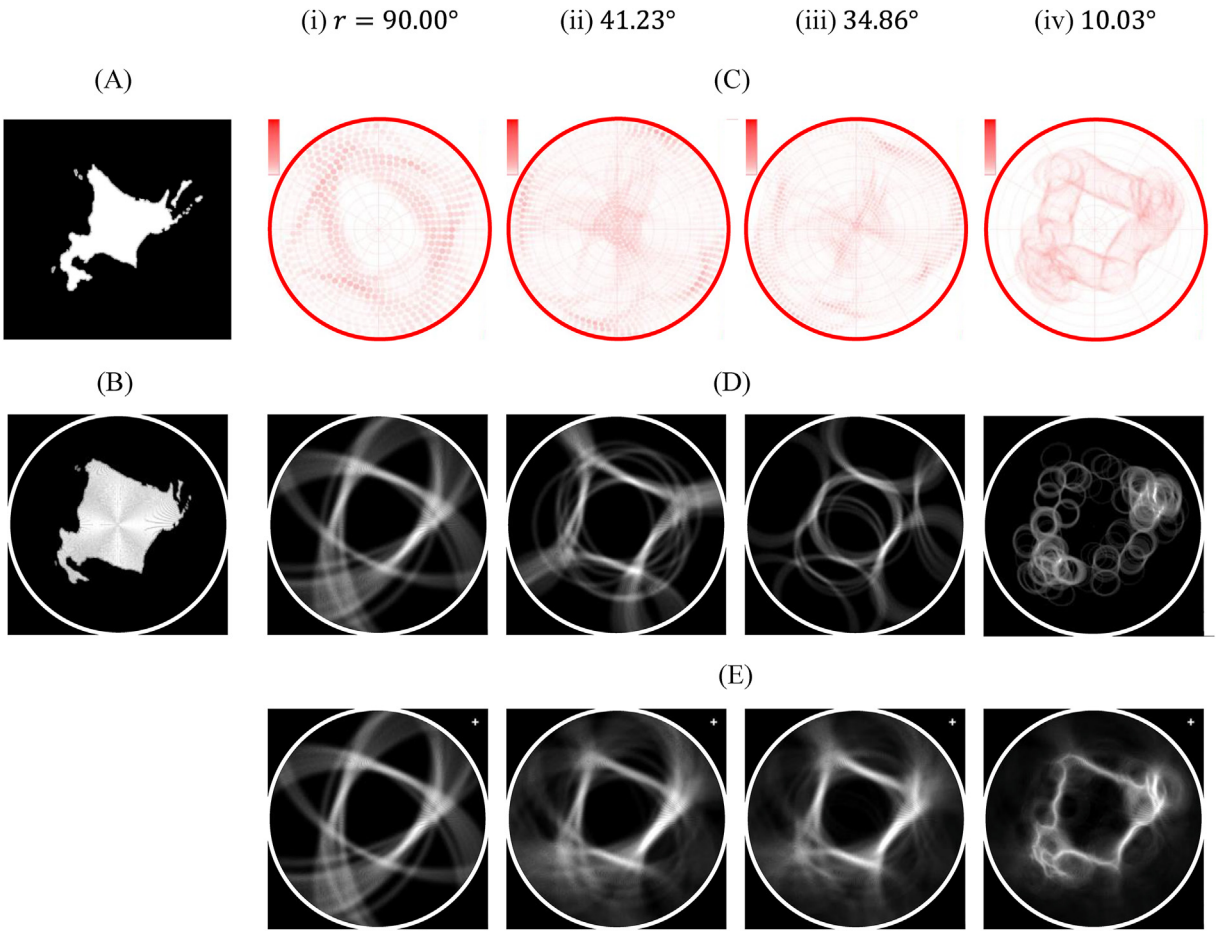

Figure 15. Responses of the CDCs to a figure composed of various curvature circles. As such figure, the silhouette of Hokkaido in Japan was used. The various curvature circles constituting this silhouette were detected separately along the r height axis of the CDC column. (A) This silhouette is shown on the plane. (B) It was projected onto the eyeball, and then was presented as a stimulus. (C) Cross-sectional responses of the CDC column to the silhouette of (B) are shown. (D) The eyeball images calculated reversely from the cross-sectional responses of (C) using the network (Figure 6) are shown. In (iii), a curvature circle inscribed in a quadrilateral that represents the outline of the silhouette was reverse-calculated. (E) Each image was obtained by accumulating the reverse-calculated images of (D) in the order (i), (ii), (iii), and (iv). This accumulation progressed as the height r became smaller, and finally, in (iv), the presented silhouette (B) was reconstructed.

(Figure 6(C)) was traced back to determine the location (ρ,θ) of an NDS simple cell. Then, from this simple cell, the network of Hough transform (Figure 6(B)(iii)) was traced back to determine the group of LGN cells on a tangent (Figure 6(B)(ii)). Since this tangent has the same position and orientation as a tangent in the retinal cell array (Figure 6(B)(i)), the tangent was drawn in the corresponding RF (Figure 6(A)). The intensity of the drawn tangent was equal to the response of this CDC cell: if the response is less than 10% of the maximum response within the CDC column, the tangent was not drawn. Performing this drawing for all CDCs in (B)(ii) causes a curve enveloped by these tangents to be formed on the eyeball (Figure 6(A)). Thus, the eyeball image in (C)(ii) was reversely calculated as this curve. Next, the eyeball image of (C)(i) was similarly calculated reversely from the cross section of (B)(i).

Thus, the above matches between the reversely calculated images (C (i and ii)) and the presented great and small circles ((A)) confirmed that the network (Figure 6) were correctly performed to detect these great and small circles.

4.3. Triangle

The simulation in Figure 13 confirmed that three types of curvature circle included in a triangle were detected separately along the r height axis of the CDC column. This detection allowed the third feature in Section 3.4 to be confirmed.

The (A) shows a triangle on a plane. The (B) shows a triangle on the eyeball obtained by projecting the triangle in (A) onto it, which was presented as a stimulus. The (C) shows the cross sections of the CDC column to the triangle of (B), and the (D) shows the eyeball images that were calculated reversely from (C) in the same way as in Figure 12(C).

The first type above is each side (i.e. each great circle) of the triangle. In (C)(i), three CDCs corresponding to these sides were activated maximally and detected them. The centers of these great circles are schematically shown on the cross section of r = 90 deg in (E). In (D)(i), the eyeball image calculated reversely from (C)(i) corresponds to the triangle of (B). The second type is a circle with a radius r of 41.23° inscribed in the triangle. In (C)(ii), a CDC corresponding to this circle was activated maximally at the disk center and detected it. The image of (D)(ii) calculated reversely from (C)(ii) corresponds to this inscribed circle. The third type is each circle with a radius r of 10.03° inscribed in two sides near each vertex. In (C)(iii), three CDCs corresponding to these circles were activated maximally and detected them. The image of (D)(iii) calculated reversely from (C)(iii) corresponds to these circles.

Summarizing the above, three types of curvature circle included in the triangle (i.e. the great circles, the circle inscribed in the triangle, and the circles inscribed in the two sides) were extracted in the order of coarse-to-fine along the r axis of the CDC column. This extraction along the height axis is consistent with the third feature in Section 3.4, and thus this feature has been confirmed.

Each image in (F) was obtained by accumulating the reverse-calculated images in (D) in the order (i), (ii), and (iii). This accumulation progressed as the height r became smaller, and finally, in (iii), the presented triangle (B) was reconstructed. Unlike (B), only the contour was reconstructed because the uniform luminance portion of (B) was lost by the DOG convolution (Figure 6(B)(ii)).

Next, Figure 14(A) shows a triangle on a plane obtained by adding fine unevenness to each side of the triangle in Figure 13(A). The (B) shows a triangle on the eyeball obtained by projecting the triangle in (A) onto it, which was presented as a stimulus. The (C) shows the cross sections of the CDC column to the triangle of (B), and the (D) shows the eyeball images that were calculated reversely from (C).

The reverse-calculated images in (D)(i and ii) are similar to those without unevennesses in Figure 13(D)(i and ii). This is because the radii r of these images (i.e. r = 90 and 41.23 deg) is much larger than the unevenness size, and thus these radii were detected as they were. On the other hand, in (D)(iii), these unevenness were detected, and many reconstructed circles occurred: their centers are schematically shown on the cross section of r = 10.03 deg in (E).

Each image in (F) was obtained by accumulating the reverse-calculated images of (D) in the order (i), (ii), and (iii). This accumulation progressed as the height r became smaller, and finally, in (iii), the presented triangle (B) was reconstructed including the features of the almost details.

4.4. Figure composed of various curvature circles

As such a figure, the silhouette of Hokkaido in Japan was used. The simulation in Figure 15 confirmed that the various curvature circles constituting this silhouette were detected separately along the r height axis of the CDC column. The simulation confirmed the second and third features in Section 3.4.

The (A) shows this silhouette on a plane, and the (B) shows a figure obtained by projecting it onto the eyeball, which was presented as a stimulus. The (C) shows the cross sections of the CDC column to the (B), and the (D) shows the eyeball images that were calculated reversely from (C) in the same way as in Figure 12(C).

The (D)(i) shows that the largest curvature circles (i.e. the great circles) were detected and thus the coarsest components (i.e. a rough outline) of the silhouette were extracted. As the height r decreased from (D)(ii) to (D)(iv), smaller curvature circles were detected and thus the finer components of the silhouette were extracted.

In this way, the various curvature circles constituting the silhouette were extracted in the order of coarse-to-fine along the r axis of the column. This extraction along the height axis is consistent with the third feature in Section 3.4, and thus this feature has been confirmed.

The (C) and (D) show that the CDCs detected not only the entire circle shown in Figures 11(A) and 12(A), but also the various circular arcs (i.e. the local contours) in (B). These have allowed the description in Section 3.3 i.e. "the CDC can detect even if the curvature circle is a circular arc" to be confirmed.

Each image in (E) was obtained by accumulating the reverse-calculated images of (D) in the order (i), (ii), (iii), and (iv). This accumulation progressed as the height r became smaller, and finally, in (iv), the presented figure (B) was reconstructed including the features of the almost details. If reverse-calculated images of (D) with a radius r less than 10.03° can be added, a more detailed reconstruction will be possible.

We show below that the two types of reconstruction are equivalent: the first type is the above reconstruction that was performed by the total accumulation of the reverse-calculated images; the second type is the reconstruction described as the second feature (Section 3.4). First, the second type is summarized. A CDC detects the parameters (i.e. the center and radius) of every curvature circle that constitutes a figure, and then a circle corresponding to these parameters is drawn on the eyeball, with its intensity equal to this CDC response. Performing this drawing for all curvature circles causes the figure to be reconstructed as an envelope of these circles. Next, the first type is summarized based on Figure 6 (Section 4.2 for details). From every CDC activated in the CDC column (Figure 6(C)), the network representing the Hough and 3D normal-line transforms (Figure 6(B(iii) and C)) is traced back to determine a tangent in the LGN cell array (Figure 6(B)(ii)). This tangent is drawn in a corresponding RF (Figure 6(A)), with its intensity equal to this CDC response. Performing this drawing for all CDCs activated in the column causes a curve enveloped by these tangents to be formed, and thus the figure is reconstructed as this curve (Figure 15(E)(iv) as an example). Compare these two reconstructions. The first type is obtained as the envelope of tangents, whereas the second type is obtained as the envelope of circles. Since each tangent is a part of the circle as shown in Figure 6(A), the first and second types are equivalent.

The first reconstruction type was confirmed by the simulation in (E)(iv), and thus based on this equivalence the second reconstruction type, which characterizes the second feature in Section 3.4, has been also confirmed.

5. Discussion

Brief overviews are provided below to highlight the content of the following subsections.

In Section 5.1, we will compare the three types of CDC modeled in Section 3 (i.e. the cells CDC(α,β,r), $CDC_{\alpha,\beta}(r)$, and $CDC_r(\alpha,\beta)$) with the actual cells in area V4. As a result, the following correspondence will be described. First, the cells $CDC_{\alpha,\beta}(r)$ and $CDC_r(\alpha,\beta)$ exhibit the same invariance and selectivity to stimuli as the position-invariant cells and curvature-invariant cells, respectively. Next, the cell $CDC_r(\alpha,\beta)$ exhibits the same preference as the cell that prefers a concentric circle. Finally, the cell CDC(α,β,r) corresponds to two types of cell: the first is the cell that responds selectively to both curvature and position of a contour; the second is the cell that exhibits a trade-off between curvature preference and position invariance. Thus, it will be shown that these three CDC types reflect the response to various stimuli in actual area V4 cells. In addition, we will make the following explanations: (1) the selective-response width $\Delta_{\alpha\beta}$ of cell CDC(α,β,r) allows the neurophysiological process why this trade-off occurs to be explained; (2) the third feature (Section 3.4) allows the coarse-to-fine response of area IT cells to be explained neurophysiologically.

In Section 5.2, we will make the following three comparisons with previous cell models and method.

First, we will compare the cell hierarchy (Figure 10) with cell models previously reported. As a result, the following correspondence and difference will be described: (1) the NDS simple cell, CDC(α,β,r), and $CDC_{\alpha,\beta}(r)$ of the hierarchy correspond to the S1, S2, and C2 cells of the above cell models, respectively; (2) this hierarchy differs most from these cell models in that the hierarchy is represented by a series of mathematical transformations that represent its networks (i.e. the Hough transform, 3D normal-line transform, and two types of positive-component accumulation).

Second, we will compare the cell CDC(α,β,r) with a cell model that responds selectively to a very local curvature (i.e. a circular arc with very small central angle) and has been named an endstopped cell. As a result, we will find the following: (1) this endstopped cell can be modeled also based on the network in Figure 6, and this modeling is equivalent to performing the curvature-circle detection (Section 3.1) for this arc with very small central angle; (2) increasing this angle until an entire circle is formed allows the cell CDC(α,β,r) to be modeled.

Third, we will compare the algorithm (i.e. the 3D normal-line transform), based on which the cell CDC(α,β,r) was modeled, with circle Hough transform (CHT) that is an engineering method for detecting circles. As a result, it will be shown that this algorithm allows the problems of the CHT to be solved.

In Section 5.3, in order to validate these three CDC types neurophysiologically, we will propose three types of experimental method using microelectrodes, where each method type uses a circle or dot or bar

stimulus. The bar stimulus will allow not only the above validation, but also the execution of the network (Figure 6) to be validated.

In Section 5.4, we will propose that the cell-array conversions, which were found in Section 3.6 and played an important role in acquiring the complex feature and the constancy, are performed commonly in the visual cortex. Making this proposal is another key point in our paper, and will be done as follows:

First, combining the above hierarchy (Figure 10; Section 3.6) with three hierarchies modeled previously, we will form four types of hierarchy, which are composed of 16 types of cell model and process both shape and space informations.

Next, we will find that these hierarchies have the following noteworthy natures: (1) each hierarchy performs a series of the above cell-array conversions; (2) each array conversion is performed by one of convolution, correlation, and pooling; (3) the convolution and correlation create new array parameters (i.e. new features) to acquire more complex features, whereas the pooling annihilates an array parameter to acquire the invariance to that parameter; (4) thus, this array conversion allows every cell in the hierarchy to acquire either more complex feature or the invariance (or the constancy).

Finally, thus, we will also find that these four hierarchies are composed of 16 types of cell-array conversion across various areas of the visual cortex, specifically, across areas LGN, V1, V2, V4, middle temporal (MT), medial superior temporal (MST), frontal eye field (FEF), and caudal intra-parietal (CIP). Based on this finding, we will propose a hypothesis that such array conversions are one of the basic functions performed across the cortex except for area IT, and are performed commonly in the cortex to play an important role in acquiring the complex feature and the constancy.

5.1. Comparison with neurophysiology

Many cells in area V4 were reported to respond selectively to the curvature κ of local contours used as stimuli. The three types of CDC modeled in Section 3 were compared below with these area V4 cells.

Before comparing, we point out that the parameter representation of local contours differs between these area V4 cells and the CDC types. In the area V4 cells, the contour was represented by its position and curvature κ, and then the selectivity and invariance of the cells for the contour were evaluated using these two parameters (Section 1). On the other hand, in the CDC types, we used the center (α,β) and radius r of a curvature circle in contact with this contour (Figure 1(A)), as the parameters: the (α,β) corresponds to the O_C in Figure 1(A), and these (α,β) and r are detected by the CDC.

The parameters of these two representations differ in this way. However, as described in Section 1, these parameters correspond to each other, in terms of the selectivity and invariance evaluations of cells to the parameters: specifically, the parameters (i.e. the curvature κ and position) of the contour correspond to those (i.e. the radius r and center (α,β)) of a curvature circle in contact with this contour, respectively. In other words, the parameters (i.e. the curvature κ and position) for evaluating area V4 cells correspond to those (i.e. the radius r and center (α,β)) for evaluating CDC types, respectively. Therefore, we can use either of these two representations to evaluate the selectivity and invariance of cells for the parameters.

The above correspondence between the curvature κ and the radius r is examined as follows. This correspondence was obtained on the plane and has a relation of $\kappa = 1/r$ (Section 1). On the other hand, the CDC detects a radius r of curvature circle on the eyeball, and thus another relation between the r and κ needs to be found on the eyeball. This relation is expressed by following equation based on the geodesic curvature (Bronshtein and Semendyayev, 1978).

$$\kappa = \cot r \tag{10}$$

This equation indicates that the curvature κ corresponds to the radius r, in terms of the selectivity and invariance evaluations to the parameters. Therefore, this correspondence on the eyeball is the same as that on the plane.

5.1.1. Position-invariant cells in area V4

Position-invariant cells, specifically, cells that responded invariant to the position of a local contour but selectively responded to its curvature κ were reported in area V4 (Pasupathy & Conner, 1999, 2001, 2002).

We show below that this area V4 cell (i.e. the position-invariant cell) corresponds to the position-invariant CDC denoted as $CDC_{\alpha,\beta}(r_0)$, which was modeled in Section 3.5.1. This cell $CDC_{\alpha,\beta}(r_0)$ responds invariant to the center (α,β) of the stimulus circle in the RF, but selectively responds to its radius r_0 (Figure 8(B)). As described above, the parameters (i.e. the position and curvature κ) for evaluating the area V4 cell correspond to those (i.e. the center (α,β) and radius r_0) for evaluating the cell $CDC_{\alpha,\beta}(r_0)$, respectively, because this $CDC_{\alpha,\beta}(r_0)$ belongs to the CDC types. Thus, this area V4 cell corresponds to the cell $CDC_{\alpha,\beta}(r_0)$, in terms of the selectivity and invariance to these parameters.

We propose that this area V4 cell is the cell $CDC_{\alpha,\beta}(r_0)$. In order to validate this proposal neurophysiologically, an experimental method using microelectrodes will be described in Section 5.3.1. We think that this method enables to validate that this area V4 cell is the cell $CDC_{\alpha,\beta}(r_0)$.

5.1.2. Curvature-invariant cells in area V4

Size-invariant (i.e. curvature-invariant) cells, specifically, cells that responded invariant to the size (i.e. the curvature κ) of a local contour but selectively responded to its position were reported in area V4 (El-Shamayleh and Pasupathy, 2016).

We show below that this area V4 cell (i.e. the curvature-invariant cell) corresponds to the curvature-invariant CDC denoted as $CDC_r(\alpha_0,\beta_0)$, which was modeled in Section 3.5.2. This cell $CDC_r(\alpha_0,\beta_0)$ responds invariant to the radius r of the stimulus circle, but selectively responds to its center (α_0,β_0) (Figure 8(C)). As described above, the parameters (i.e. the curvature κ and position) for evaluating the area V4 cell correspond to those (i.e. the radius r and center (α_0,β_0)) for evaluating the cell $CDC_r(\alpha_0,\beta_0)$, respectively. Thus, this area V4 cell corresponds to the cell $CDC_r(\alpha_0,\beta_0)$, in terms of the selectivity and invariance to these parameters.

In addition, cells that responded intensively to concentric circles were reported in area V4 (Gallant et al., 1993, 1996; Dumoulin and Hess, 2007). The cell $CDC_r(\alpha_0,\beta_0)$ also responds intensively to this concentric circle (Section 3.5.2). Thus, this area V4 cell corresponds to the cell $CDC_r(\alpha_0,\beta_0)$.

Based on these correspondences, we propose that the cell $CDC_r(\alpha_0,\beta_0)$ is both of these two types of area V4 cell: i.e. the curvature-invariant cell and the cell responding to the concentric circle. In order to validate this proposal neurophysiologically, an experimental method using microelectrodes will be described in Section 5.3.1. We think that this method enables to validate that these two area V4 cells are the cell $CDC_r(\alpha_0,\beta_0)$.

5.1.3. Trade-off cells in area V4

Cells that exhibited a trade-off between curvature preference and position invariance were reported in area V4 (Nandy et al., 2013; Sharpee et al., 2013; Pasupathy and Conner, 1999): specifically, this trade-off exhibits that a cell preferring high curvature has low position invariance, while a cell preferring low curvature has high position invariance.

We show below that this trade-off cell corresponds to the cell $CDC(\alpha_0,\beta_0,r_0)$, which was modeled in Section 3.1. First, this cell $CDC(\alpha_0,\beta_0,r_0)$ responds selectively to both center (α_0,β_0) and radius r_0 of a

stimulus circle (Figure 8(A)). The width $\Delta_{\alpha\beta}$ of this selective response at (α_0,β_0) is expressed as $\Delta_{\alpha\beta} = (\Delta\theta_{SC}/2)$ sin r by Eq. (6): the $\Delta\theta_{SC}$ represents the discrimination in θ orientation of an NDS simple cell (Appendix C), and the r represents the radius of the circle. Since the curvature κ is expressed as $\kappa = \cot r$ by Eq. (10), the following equation is obtained by substituting these equations.

$$\Delta_{\alpha\beta} = (\Delta\theta_{SC}/2) \sin(\tan^{-1}(1/\kappa)) \quad (11)$$

Next, this width $\Delta_{\alpha\beta}$ corresponds to the above position invariance: this is because, as shown in Figure 8(A)(i), the response of the cell $CDC(\alpha_0,\beta_0,r_0)$ does not change even if the center position (α_0,β_0) of the circle translates within the width $\Delta_{\alpha\beta}$. Thus, this equation represents the relationship between the position invariance $\Delta_{\alpha\beta}$ and the curvature κ.

Thus, this equation means that a CDC with large κ (i.e. a CDC preferring high curvature) has low position invariance $\Delta_{\alpha\beta}$, while a CDC with small κ (i.e. a CDC preferring low curvature) has high position invariance $\Delta_{\alpha\beta}$. This nature of the CDC is the same as that of the above trade-off cell. Therefore, this cell $CDC(\alpha_0,\beta_0,r_0)$ corresponds to the trade-off cell.

In this way, the discrimination threshold $\Delta_{\alpha\beta}$ expressed by Eq. (6) (i.e. the selective-response width $\Delta_{\alpha\beta}$ of cell $CDC(\alpha,\beta,r)$) allows the neurophysiological process of this trade-off to be explained, and thus this trade-off has been clarified to result from the RF structure of NDS simple cell (Figure C1(A) in Appendix C). We point out that the cell $CDC_r(\alpha_0,\beta_0)$ also exhibits this trade-off.

In addition, a cell type that responded selectively to both curvature κ and position of a local contour and was named a absolute cell was reported in area V4 (El-Shamayleh and Pasupathy, 2016). We show that this absolute cell corresponds to the cell $CDC(\alpha_0,\beta_0,r_0)$, as follows. The cell $CDC(\alpha_0,\beta_0,r_0)$ responds both center (α_0,β_0) and radius r_0 of a stimulus circle (Figure 8(A)). As described above, the parameters (i.e. the curvature κ and position) for evaluating the absolute cell correspond to those (i.e. the radius r_0 and center (α_0,β_0)) for evaluating the cell $CDC(\alpha_0,\beta_0,r_0)$, respectively. Thus, this absolute cell corresponds to the cell $CDC(\alpha_0,\beta_0,r_0)$.

Based on these correspondences, we propose that the cell $CDC(\alpha_0,\beta_0,r_0)$ is both of the trade-off cell and the absolute cell. In order to validate this proposal neurophysiologically, three types of experimental method using microelectrodes will be described in Section 5.3. We think that these method types enable to validate that these two area V4 cells are the cell $CDC(\alpha_0,\beta_0,r_0)$.

5.1.4. Cells exhibiting coarse-to-fine responses in area IT

Cells that exhibited the coarse-to-fine responses were reported in area IT (Sugase et al., 1999; Tamura and Tanaka, 2001): specifically, these cells responded first to coarse (or global) components of stimuli and then responded to their fine components with average delay of 51 ms. These cells were thought to process low spatial frequency components first and then high spatial frequency components (Bar 2003; Hughes et al., 1996).

We show as follows that this coarse-to-fine response can be explained by the third feature described in Section 3.4. First, this feature causes the CDCs in area V4 to extract components of the stimuli in the order of coarse-to-fine along the r height axis of the CDC column. Next, this causes the following in area IT: (1) these CDCs deliver to area IT first the extracted coarse components and then deliver the extracted fine components; this can be done by first delivering an information of the higher cross section of the column and then delivering that of its lower cross section (Figure 7); (2) by this delivery, area IT cells exhibit the coarse-to-fine response described above. Thus, the third feature performing this extraction allows the coarse-to-fine response of area IT cells to be explained. We point out that the cell $CDC_{\alpha,\beta}(r)$ having the r height coordinate also can perform this extraction as well as the cell $CDC(\alpha,\beta,r)$ (Section 3.6), and thus causes area IT cells to also perform the coarse-to-fine response.

We think that this coarse-to-fine response in area IT enable the following perception: the outline of a figure that is composed of the coarse components is perceived first, and then its details that is composed of the fine components is identified.

5.2. Comparison with previous models

5.2.1. Neurophysiological models

A hierarchy composed of S1, C1, S2, and C2 cells was reported (Cadieu et al, 2004, 2007; Riesenhuber and Poggio, 1999; Schneider and Riesenhuber, 2002; Serre et al., 2007). The S1 cell corresponds to a simple cell in area V1, its RF was given as a Gabor function, and the cell response was modeled as a convolution (or a dot product or a template match) between responses of retinal cells and this Gabor function. The C1 cell corresponds to a complex cell in area V1, and the cell response was modeled as a max-pooling of the S1 cell responses preferring the same orientation. The S2 cell responds selectively to both curvature κ and the position of a local contour, and the cell response was modeled as a convolution between the C1 cell responses and a synaptic weight matrix that was determined by training. The C2 cell responds invariant to the position of the contour but selectively respond to its curvature, and the cell response was modeled as a max-pooling of the S2 cell responses preferring the same curvature.

This hierarchy is compared with that shown in Figure 10, as follows, in which the LGN and NDS simple cells were modeled previously (Kawakami and Okamoto, 1996; Kawakami, 1996) and the three types of CDC were modeled in Section 3.

First, the S1 cell corresponds to the NDS simple cell denoted as $SC_{NDS}(\rho,\theta)$ that performs the Hough transformation of LGN cell responses. The differences between them are as follows. The RF of S1 cell was given as the Gabor function, but it is considered to be not clear why the cell has a Gabor-shaped RF. On the other hand, the cell $SC_{NDS}(\rho,\theta)$ possessed a Gabor-shaped RF (Figures 15 and 16 of Kawakami and Okamoto (1996)): this is because the Hough transformation of the DOG function, which represents the RF of the LGN cell, causes an RF very similar to the Gabor function to be formed. Thus, it has been clarified that this Gabor-shaped RF results from the Hough transformation of the DOG function.

Second, we modeled a complex cell corresponding to the C1 cell as an accumulation (i.e. a type of pooling) of the cell responses $SC_{NDS}(\rho,\theta)$ preferring the same θ orientation, but this complex cell was not shown in Figure 10 because it was not used to model the CDC.

Third, the S2 cell corresponds to the cell $CDC(\alpha,\beta,r)$, as follows. The S2 cell responds selectively to both curvature κ and position of a local contour, whereas as shown in Figure 8(A) the cell $CDC(\alpha,\beta,r)$ responds selectively to both radius r and center (α,β) of the curvature circle in contact with this contour. As described in 5.1, the parameters (i.e. the curvature κ and position) for evaluating the S2 cell correspond to those (i.e. the radius r and center (α,β)) for evaluating the cell $CDC(\alpha,\beta,r)$, respectively. Thus, this S2 cell corresponds to the cell $CDC(\alpha,\beta,r)$, in terms of the selectivity and invariance to these parameters.

There are two differences between the S2 cell and the cell $CDC(\alpha,\beta,r)$. The first difference is that the cell $CDC(\alpha,\beta,r)$ detects both an entire circle and a local contour (i.e. a part of the circle) (Section 3.3), whereas the S2 cell detects (or responds to) the local contour. The second difference is whether training is necessary or not. In the S2 cell, the synaptic weight matrix is determined by training, as described above. On the other hand, in the cell $CDC(\alpha,\beta,r)$, this matrix is determined by the 3D normal-line transform (Section 3.1), and thus there is no need for training. This matrix is considered to correspond to the matrix obtained after the above training of the S2 cell has been performed for a circle and it has converged.

Fourth, the C2 cell corresponds to the cell $CDC_{\alpha,\beta}(r)$. The difference is the way of pooling. The C2 cell uses the max-pooling, whereas the cell $CDC_{\alpha,\beta}(r)$ uses the positive-component accumulation (Eq. (8)) that is considered to correspond to a global average pooling.

The above is summarized. The cells $SC_{NDS}(\rho,\theta)$, $CDC(\alpha,\beta,r)$, and $CDC_{\alpha,\beta}(r)$ correspond to the S1, S2, and C2 cells, respectively, with some differences described above. This hierarchy differs most from the above Cadieu et al.'s cell models in that the hierarchy is represented by a series of mathematical transformations that represent its networks (Section 3.6): the Hough transform, 3D normal-line transform, and two types of positive-component accumulation.

In addition, a cell that responds selectively to a very local curvature (i.e. a circular arc with very small central angle) and was named an endstopped cell was modeled by combining the simple and complex cells (Rodriguez-Sanchez and Tsotsos, 2012). These endstopped cells were further combined to model a cell that responds selectively to both position and curvature of a local contour. This cell corresponds to the cell CDC (α,β,r) for the same reason as above S2 cell.

This endstopped cell can be modeled also based on the network (Figure 6), as follows. Assuming this arc of the curvature circle in Figure 6(A), pick up RFs overlapping with the arc. In each RF, a tangent (Figure 6(B)(i)) in contact with this arc is detected by an NDS simple cell in Figure 6(B)(iii). Next, this simple cell is connected to all CDCs on a 3D normal-line in the CDC column (Figure 6(C)), and then this connection (i.e. this network) causes the simple cell to fire all CDCs on the 3D normal line. Performing this connection for all RFs on the arc causes a CDC at the intersection of these normal lines to fire most intensively (Figure 4(B)), and thus this CDC can detect this arc as the coordinates of this intersection. This CDC detecting the arc corresponds to the endstopped cell, and thus the endstopped cell has been modeled using the network (Figure 6). This modeling is equivalent to performing the curvature-circle detection (Section 3.1) for this arc with very small central angle.

Increasing the central angle of this arc allows the above cell, which was obtained by combining these endstopped cell, to be modeled. Further increasing this angle until an entire circle is formed allows the cell CDC (α,β,r) to be modeled.

5.2.2. Engineering method

Circle Hough transform (CHT) was proposed as an engineering method for detecting a circle (Duda and Hart, 1972; Illingworth and Kittler, 1987). After that, randomized Hough transform (RHT) has been studied for speeding up and precision improvement (Xu et al., 1990; Chen and Chung, 2001; De Marco et al., 2015). The CHT that is the origin of RHT is compared below with our algorithm (Section 2).

The CHT uses the rectangular solid (x,y,r) in Figure 2(A). Giving on a plane a circle with a radius r = 60 using four points on its circumference, this solid was cut at each height r and its cross section (x,y) was arranged in Figure 16(A). In (iv), the given four points form a circle with a radius of 60 which corresponds to the given circle, and this circle is shown in each cross section as dotted lines for reference. As shown in (iii) as an example, in a cross section of any height r, a circle with the radius r centered at each given point is drawn. This circle drawing is a feature of the CHT. These circles increase in size with height r and then intersect at one point in (ii). The center and radius of the given circle are detected as the coordinates of this intersection.

Our algorithm uses the cylinder (α,β,r) in Figure 4(A). Giving on the eyeball a circle with a radius r = 60 deg using four tangents and contacts on its circumference, this cylinder was cut at each height r and its cross section (α,β) was arranged in Figure 16(B). In (iv), the given four contacts form a circle with a radius of 60° which corresponds to the given circle, and this circle is shown in each cross section as dotted lines for reference. As shown in (iii) as an example, in a cross section of any height r, each given contact shifts inward by r along a normal line. This shift is a feature of our algorithm. The shift results from the V shape of the 3D normal line (Figure 4(A)): this is because when the height increases by r from the bottom, the intersection of this V-shape and the cross section shifts by r from the contact (Section 2.2.2). This shift increases with r, and then the shifted contacts converge to one point at (ii). The center and radius of the

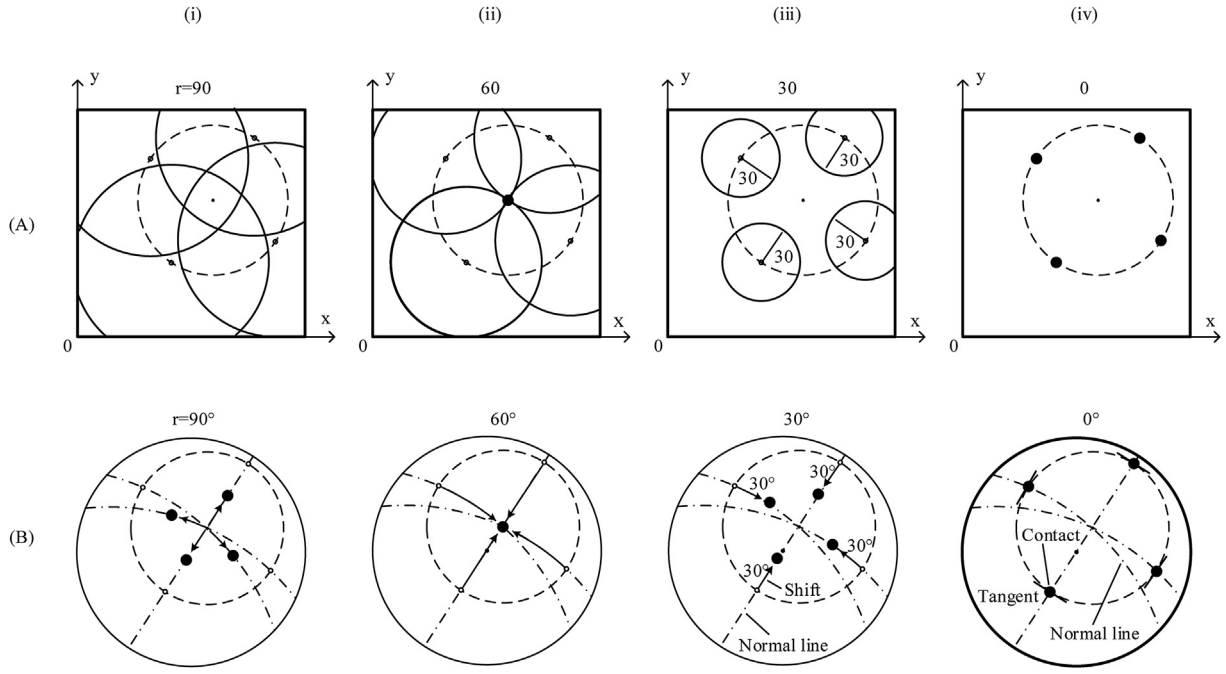

Figure 16. Comparison of our algorithm with CHT. CHT was proposed as an engineering method for detecting a circle (Duda and Hart, 1972; Illingworth and Kittler, 1987). This CHT was compared with our algorithm (Section 2). (A) The CHT uses the rectangular solid (x,y,r) in Figure 2(A). Giving on a plane a circle with a radius r = 60 using four points on its circumference, this solid was cut at each height r, and its cross section (x,y) was arranged. As shown in (iii) as an example, in a cross section of any height r, a circle with a radius r centered at each given point is drawn. This circle drawing is a feature of the CHT. This circle increases in size with height r and then intersect at one point in (ii). Thus, the center and radius of the given circle have been detected as the coordinates of this intersection. (B) Our algorithm uses the cylinder (α,β,r) in Figure 4(A). Giving on the eyeball a circle with a radius r = 60 deg using four tangents and contacts on its circumference, this cylinder was cut at each height r, and its cross section (α,β) was arranged. As shown in (iii) as an example, in a cross section of any height r, each given contact shifts inward by r along a normal line. This shift is a feature of our algorithm. This shift increases with r, and then converges to one point at (ii). Thus, the center and radius of the given circle have been detected as the coordinates of this convergence point.

given circle are detected as the coordinates of this convergence point. Note that the shift to the outside is omitted for ease of viewing. This figure is the same as Figure 5 except that the number of contacts and tangents and the radius are different.

Our algorithm has two features compared to the CHT. The first feature is the ability to process an arbitrary figure in space composed of straight lines and curves using only circles on the eyeball (Section 3.4). This feature results from the projection onto the eyeball: this is because any straight line in space is transformed to a great circle on the eyeball by this projection, and thus it can be processed as a kind of circle. On the other hand, the CHT can not detect a straight line that represents a circle with an infinite radius.

The second feature is the ability to perform the sharp circle detection, as follows. The CHT has the following weaknesses that make it difficult to perform a sharp circle detection. Focus on the (A)(ii) in which the detection is performed. Although four circles intersect at one point, in the actual circle detection, more than 100 circles intersect at this point. Thus, a wide range around this intersection is covered by these overlapping circles. This overlap causes the accumulative responses at the intersection to become broad, and thus a sharp circle detection is difficult to be performed. On the other hand, in our algorithm, this accumulation is performed only at one point ((B)(ii)), and thus no overlap like CHT occurs. Therefore, a sharp circle detection can be performed. This difference between the CHT and our algorithm is due to the following: in the CHT, each point on the circumference is converted to a circle, whereas in our algorithm, as described above, each point shifts as it is.

In this way, this algorithm solves the above problem of CHT, and thus the CDC modeled based on the algorithm can perform better curvature-circle detection than CHT.

5.3. Proposal of experimental method for validating CDCs

In order to validate the three types of CDC (i.e. CDC(α,β,r), $CDC_{α,β}(r)$, and $CDC_r(α,β)$) neurophysiologically, we propose experimental methods using a microelectrode. A microelectrode is inserted in the vicinity of a cell in area V4 of a monkey and then its extracellular responses to three types of visual stimulus (i.e. a circle, dot, and bar) are recorded. To validate cell CDC(α,β,r), perform the above recording also for cells in area V2 (Section 5.4.1.1 described later).

5.3.1. Circle stimuli

As a stimulus, a circle with its radius r and center (α,β) is presented on the eyeball, and the cell response to it is recorded. Then, this response is voted for a position (α,β,r) in the cylinder (Figure 17). Performing this vote for all r and (α,β) will causes one of three types of pattern to occur in the cylinder, as follows.

If a pattern of (A) that has a selectivity to a position $(α_0,β_0,r_0)$ occurs in the cylinder, this recorded cell is validated to be the cell $CDC(α_0,β_0,r_0)$ that detects a circle with the center $(α_0,β_0)$ and radius r_0. This is because the selectivity in (A) corresponds to that of the cell $CDC(α_0,β_0,r_0)$ shown in Figure 8(A).

If a pattern of (B) that has a selectivity to a height r_0 and an invariance to every position (α,β) in the RF occurs in the cylinder, this recorded cell is validated to be the cell $CDC_{α,β}(r_0)$ that detects a circle with the radius r_0 independently of its center (α,β). This is because the selectivity and invariance in (B) correspond to those of the cell $CDC_{α,β}(r_0)$ shown in Figure 8(B).

If a pattern of (C) that has a selectivity to a position $(α_0,β_0)$ and an invariance to a height r occurs in the cylinder, this recorded cell is validated to be the cell $CDC_r(α_0,β_0)$ that detects a circle with the center $(α_0,β_0)$ independently of its radius r. This is because the selectivity and invariance in (C) correspond to those of the cell $CDC_r(α_0,β_0)$ shown in Figure 8(C). The width $Δ_{αβ}$ of this selectivity corresponds to the width $Δ_{αβ}$ of cell response (Figure 8(C)(i)), and is expressed by Eq. (6).

We note that the presentation of stimuli and the recording of cell responses, described above, can be efficiently performed using the reverse correlation technique (Jones and Palmer, 1987).

5.3.2. Dot stimuli

The eyeball in Figure 18(A) shows the equidistant projection (Figure 4(C)) of the eyeball surface onto the disk, where O corresponds to the center of the visual field. A dot stimulus (●) is presented at a position (α,β) on the eyeball, and the cell response to it is recorded. Then, this response is voted for a position (α,β) on this disk. Performing this vote for all positions (α,β) will generate a ring-like pattern, whose center and radius are $(α_0,β_0)$ and r_0 respectively, only for the cell CDC(α,β,r): the width of this ring is the $Δ_{αβ}$ represented by Eq. (6). Thus, this recorded cell is validated to be the cell $CDC(α_0,β_0,r_0)$ that detects the circle corresponding to this pattern.

5.3.3. Bar stimuli

A method for validating the network (Figure 6) is proposed in Figure 18(B) using bar stimuli. This method is performed in two steps.

In the first step, a bar with the orientation θ and position (α,β) is presented on the eyeball as a stimulus, and the cell response to it is recorded. Then, this bar is drawn on the disk of (B), with its intensity equal to the cell response. Performing this drawing for all θ and (α,β) will generate a ring-like envelope composed of the bars, only for the cell CDC(α,β,r): the center and radius of this ring are $(α_0,β_0)$ and r_0,

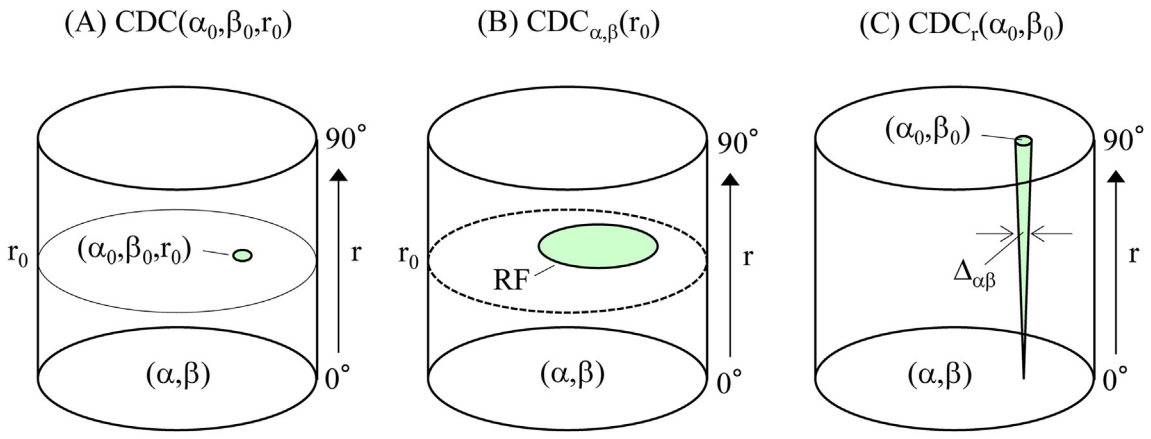

Figure 17. Experimental method for validating CDCs using circle stimuli. As a stimulus, a circle with the radius r and center (α,β) is presented on the eyeball, and the cell response to it is recorded. Then, this response is voted for a position (α,β,r) in the cylinder. Performing this voting for all r and (α,β) causes one of three types of pattern to occur in the cylinder. If a pattern (A) or (B) or (C) occurs, this recorded cell is validated to be a cell $CDC(α_0,β_0,r_0)$ or $CDC_{α,β}(r_0)$ or $CDC_r(α_0,β_0)$, respectively.

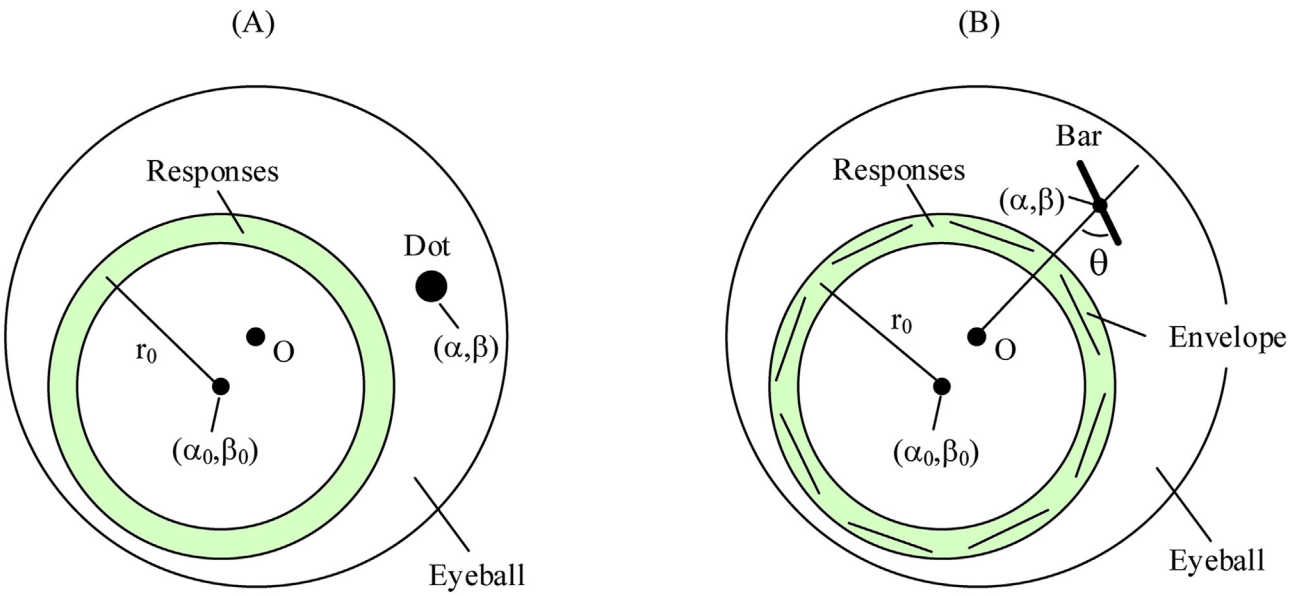

Figure 18. Experimental methods for validating CDCs using dot and bar stimuli. The disk labeled "eyeball" shows the equidistant projection of the eyeball surface (Figure 4(C)), where O corresponds to the center of the visual field. (A) The cell response to the dot stimulus with a position (α,β) on the eyeball is recorded and then voted for the position (α,β) on the disk. Performing this voting by changing the (α,β) of this stimulus causes a ring-like pattern of cell responses, whose center and radius are (α_0,β_0) and r_0, to occurs only for the cell CDC(α_0,β_0,r_0). This pattern validates this recorded cell to be the cell CDC (α_0,β_0,r_0). (B) A method for validating the network (Figure 6) that detects curvature circles is shown. This method is performed in two steps. In the first step, a bar with the orientation θ and position (α,β) is presented on the eyeball as a stimulus, and the cell response to it is recorded. Then, this bar is drawn on the disk, with its intensity equal to the cell response. Performing this drawing for all θ and (α,β) produces a ring-like envelope composed of the bars, only for the cell CDC (α_0,β_0,r_0): the center and radius of this ring are (α_0,β_0) and r_0, respectively. Thus, this ring validates this recorded cell to be the cell CDC(α_0,β_0,r_0) that detects the circle corresponding to this ring. In the second step, this ring can be constructed by tracing back the network (Figure 6) from the cell CDC(α_0,β_0,r_0) validated above, and thus confirming the coincidence between this constructed ring and the ring in (B) allows the execution of this network to be validated.

respectively, and its width is the $\Delta_{\alpha\beta}$ represented by Eq. (6). Thus, this recorded cell is validated to be the cell CDC(α_0,β_0,r_0) that detects the circle corresponding to the ring.

In the second step, we clarify below that this ring can be constructed by tracing back the network (Figure 6) from the cell CDC(α_0,β_0,r_0) validated above, using a computer simulation. If we can confirm that this constructed ring coincides with the ring in (B), the execution of this network will be validated. This construction is done as follows.

First, let us determine each bar constituting this ring, as follows: (1) Assume an RF on the eyeball (Figure 6(A)); (2) at first, by tracing back the network of the 3D normal-line transform (Figure 6(C)) from this cell CDC(α_0,β_0,r_0), determine each NDS simple cell at a location (ρ,θ) (Figure 6(B)(iii)); (3) then, by tracing back the network of Hough transform (Figure 6(B)(iii)) from this simple cell, determine a tangent in the LGN cell array (Figure 6(B)(ii)); (4) draw this tangent within the above RF (Figure 6(A)); (5) this drawn tangent is each bar constituting the ring in (B), and thus the above bar has been determined.

Next, drawing this tangent for all RFs on the eyeball causes a ring to be constructed as an envelope of these tangents. Thus, confirming the coincidence of this constructed ring with the ring in (B) allows the execution of this network to be validated.

5.4. Hierarchies of cell models

It is described below that 16 types of cell-array conversions are performed in four hierarchies of cell models across various areas of the visual cortex.

5.4.1. Cell-array conversions

We found an interesting nature of the hierarchy in Figure 10, as described in Section 3.6: specifically, this hierarchy performs a series of cell-array conversions to acquire complex features that belong to shape information; this acquisition plays an important role in shape recognition. In addition, we also found that the other hierarchy, which was modeled previously (Kawakami et al., 2000, 2003, 2010; Okamoto, 2006), performs such array conversions to acquire spatial information: this acquisition plays an important role in space recognition.

Therefore, we have merged these hierarchies into a new hierarchy of Figure 19 to generalize and describe these array conversions: this hierarchy enables to handle both shape and space informations. Figure 19 is composed of the following two sub-hierarchies. The first hierarchy shown as the green and red rectangles represents the hierarchy in Figure 10, and is related to shape recognition because it detects curvature circles constituting an arbitrary figure: this hierarchy will be described in Section 5.4.1.1. The second hierarchy shown as the blue rectangles in Figure 19(B) is related to space recognition because it detects a planar surface (or a plane) in space with motion stereo: this hierarchy will be described in Section 5.4.1.2.

Based on these sub-hierarchies, the generalized description of the array conversions above will be given in Section 5.4.1.3, where it will be shown that these array conversions are performed commonly in the visual cortex.

The outline of Figure 19 is described as follows.

Figure 19 related to both shape and space recognitions consists of the following groups of cells: (1) cells performing the preprocessings which are shown as green rectangles; (2) three types of CDC related to shape recognition which are shown as red rectangles; (3) cells related to space recognition which are shown as blue rectangles.

The three CDC types in Figure 19(A) contribute for recognizing "what we see ?": we call them the "what" cells. The two types of cell (i.e. SDC(α_S,β_S,t) and SDC(α_S,β_S,d)) in Figure 19(B) contribute for our spatial understanding of "where we are ? and how we guide movement in

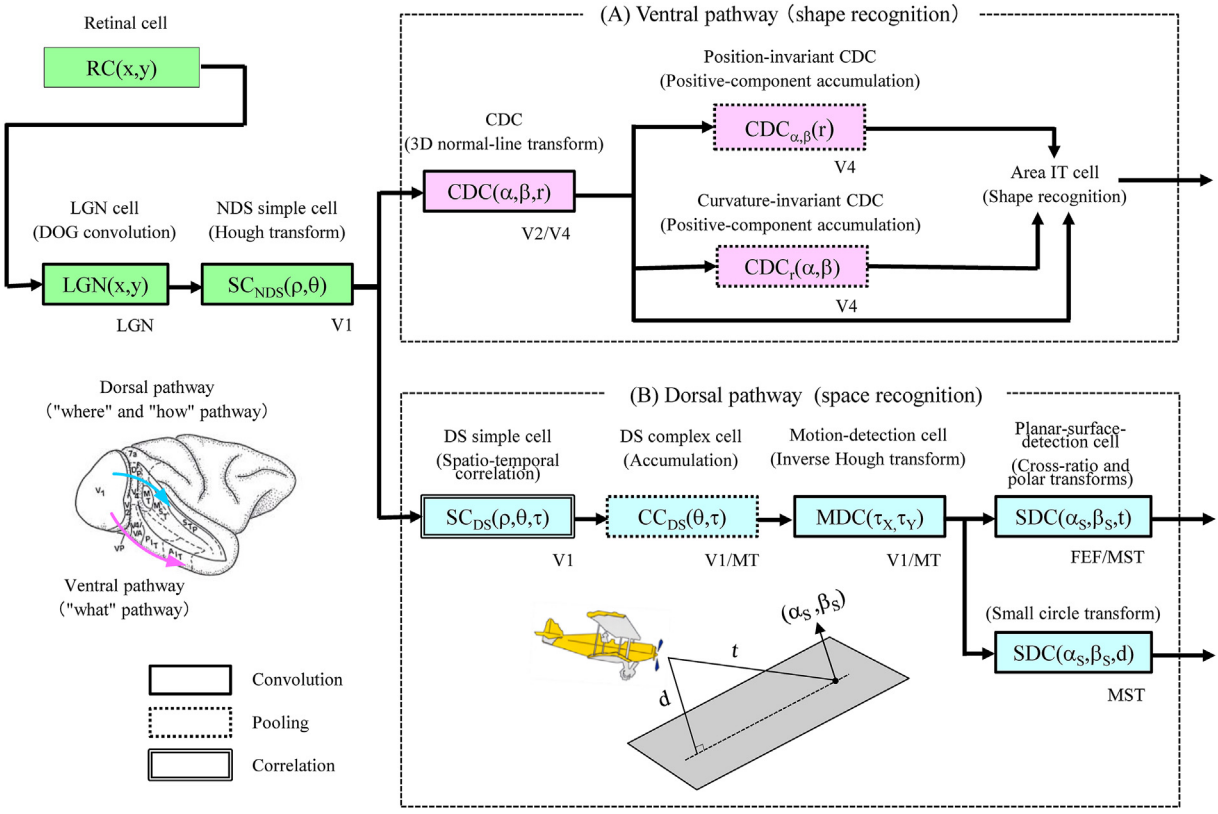

Figure 19. A hierarchy composed of two types of sub-hierarchies. The first sub-hierarchy shown as the green and red rectangles is related to shape recognition, and represents the hierarchy in Figure 10. The second sub-hierarchy shown as blue rectangles is related to space recognition. (A) The three types of CDC detect the parameters of a curvature circle: specifically, a cell CDC(α,β,r) detects both center (α,β) and radius r of the circle, a cell $CDC_{\alpha,\beta}(r)$ detects its radius r independently of its center (α,β), and a cell $CDC_r(\alpha,\beta)$ detects its center (α,β) independently of its radius r. These CDC types perform the 3D normal-line transform, the positive-component accumulation (i.e. a type of pooling) of the cell responses CDC(α,β,r) preferring the same r radius, and that preferring the same (α,β) center, respectively. (B) This second sub-hierarchy, which detects a spatial information of planes by motion stereo, was previously modeled (Kawakami et al., 2000, 2003, 2010; Okamoto, 2006), as follows. First, a series of cells (i.e. the DS simple, DS complex, and motion-detection cells) was modeled using the spatio-temporal correlation, accumulation (i.e. a type of pooling), and inverse Hough transform, respectively, to detect a local image motion (τ_X,τ_Y) in each RF. Next, these motions are integrated over all RFs on the eyeball to form an optical flow field. Finally, a planar-surface-detection cell denoted as $SDC(\alpha_S,\beta_S,t)$ (or $SDC(\alpha_S,\beta_S,d)$) extracts this flow field to detect the spatial information of a plane. This information is composed of three parameters of the time-to-contact t and shortest distance d to the plane and its 3D orientation (α_S,β_S): this time t is normalized by the fixed time delay t_d of lagged LGN cells, and this distance d is normalized by a distance traveled during the time t_d. This cell $SDC(\alpha_S,\beta_S,t)$ (or $SDC(\alpha_S,\beta_S,d)$) was modeled as a combination of the cross-ratio and polar transformations (or as the small-circle transformation) of the cell responses $MDC(\tau_X,\tau_Y)$, respectively: this cell can also be modeled as a convolution between the cell responses $MDC(\tau_X,\tau_Y)$ and a synaptic weight matrix that represents the above combination (or the small-circle transform). Using this spatial information, we can land an airplane on the runway as follows. Predicting the time t and distance d to the runway allows us to maneuver the attitude of the airplane so as to be orthogonal to the orientation (α_S,β_S) of the runway and then to land it. The cell $SC_{DS}(\rho,\theta,\tau)$ exists in area V1, and the cells $CC_{DS}(\theta,\tau)$ and $MDC(\tau_X,\tau_Y)$ exist in both area V1 and the middle temporal area (MT) (Kawakami and Okamoto, 1996; Kawakami, 1996; Okamoto et al., 1999). The cells $SDC(\alpha_S,\beta_S,t)$ and $SDC(\alpha_S,\beta_S,d)$ exist in the frontal eye field area (FEF) and medial superior temporal area (MST), respectively (Fujiwara et al., 2014).

relation to our environment ?": we call them the "where" and "how" cells, respectively. If a cell type that associates the "what" cell with the "where" and "how" cells is found in the future, these five cell types may contribute for allowing a high-order recognition such as "what is where ?" and "what and how to avoid ?": this recognition is performed by a combination of the shape and space recognitions.

Note that the LGN(x,y), $SC_{NDS}(\rho,\theta)$, and CDC(α,β,r) etc. respectively represent not only the LGN cell, NDS simple cell, and CDC etc. but also their arrays or their responses.

5.4.1.1. *Cell hierarchy for detecting curvature circles.*

This hierarchy is the first sub-hierarchy in Figure 19, and is shown as the green and red rectangles: it represents the hierarchy in Figure 10. The three types of CDC (Figure 19(A)) detect the parameters of each curvature circle constituting an arbitrary figure (Sections 3.1 and 3.5): specifically, a cell CDC(α,β,r) detects both center (α,β) and radius r of this circle, a cell $CDC_{\alpha,\beta}(r)$ detects its radius r independently of its center (α,β), and a cell $CDC_r(\alpha,\beta)$ detects its center (α,β) independently of its radius r.

These CDC types, which detect the information (i.e. the center and radius) of this circle, deliver it to area IT cells for shape recognition.

These three CDC types exist in area V4 based on the above comparison with the neurophysiological experiments (Section 5.1). We think that the cell CDC(α,β,r) also exist in area V2 based on the neurophysiological experiments (Ito and Komatsu, 2004; Ito and Goda, 2011; Hegde and Van Essen, 2000).

5.4.1.2. *Cell hierarchy for detecting planes in space with motion stereo.*

This hierarchy is the second sub-hierarchy in Figure 19, and is shown as the blue rectangles. The NDS simple cell shown as a green rectangle delivers its information not only to the cell CDC(α,β,r) in Figure 19(A) but also to this hierarchy. A series of cells in the hierarchy, which detects a planar surface (or a plane) in space with motion stereo, were previously modeled, as follows.

First, a series of cells (i.e. the directionally selective (DS) simple, DS complex, and motion-detection cells) was modeled using the spatio-temporal correlation, accumulation, and inverse Hough transform, respectively, to detect a local image motion in each RF (Kawakami and Okamoto, 1996; Kawakami, 1996; Okamoto et al., 1999): these three cell types reflect the response to various stimuli in actual cells. Next, these local motions are integrated over all RFs on the eyeball to form an optical flow field that was proposed by Gibson (1950). Finally, a planar-surface-detection cell (SDC) denoted as SDC(α_S,β_S,t) (or SDC(α_S,β_S,d)) extracts this flow field to detect the spatial information of a plane (Kawakami et al., 2000, 2003, 2010; Okamoto, 2006): note that in the above previous paper this SDC was named the MST cell. This information is composed of three parameters of the time-to-contact t and shortest distance d to the plane and its 3D orientation (α_S,β_S), where these parameters are illustrated in Figure 19(B). The arrangements in arrays of the above cell series were concretely shown in Figure 10 of Kawakami et al. (2000, 2003), including the network connecting the cells.

This hierarchy plays an important role in space recognition, as follows: specifically, using this spatial information, we can perform actions to adapt to the environment and actions to avoid it. First, we can land an airplane on the runway (see the picture of landing in Figure 19(B)): predicting the time t and distance d to the runway allows us to maneuver the attitude of the airplane so as to be orthogonal to the orientation (α_S,β_S) of the runway and then to land it. This landing has allowed the psychological finding of Gibson (1950, 1979) to be explained neurophysiologically: Gibson found that this landing is performed based on the optical flow field. Next, in daily life, the obstacle avoidance using this spatial information is important, and is performed as follows. Predicting the time t to an obstacle such as a wall (which is a vertical plane) allows us to avoid the wall to a direction orthogonal to its orientation (α_S,β_S) and then to move parallel along the wall while perceiving the distance d to it: this wall avoidance was concretely illustrated in Figure 7 in Kawakami et al. (2002).

In this way, this hierarchy detects the spatial information related to "where" and "how", where the t and d are related to "where", and the (α_S,β_S) is related to "how".

This cell SDC(α_S,β_S,t), which detects the time-to-contact t, reflects the response to various stimuli in actual cells in the frontal eye field area (FEF) of monkeys (Fujiwara et al., 2014) and in the nucleus rotundus of pigeons (Wang and Frost, 1992), and this cell response allows animal ecologies of gannets and flies (Lee and Reddish, 1981; Wagner, 1982) to be explained neurophysiologically. In addition, the cell SDC(α_S,β_S,d), which detects the shortest distance d, reflects the response to various stimuli in actual cells in the medial superior temporal area (MST) of monkeys (Fujiwara et al., 2014) and in the thalamus of pigeons (Liu et al., 2008).

We point out that this cell SDC(α_S,β_S,t) uses the same column as the cell CDC(α,β,r) in Figure 6(C): this is because both are projecting on the eyeball (Section 2.2.1). It is noteworthy that the cell SDC(α_S,β_S,t) related to space recognition uses the same column as the cell CDC(α,β,r) related to shape recognition. The difference between these cell types lies in the parameters of the column and the transforms performed in the column, as follows. First, the column parameters of SDC(α_S,β_S,t) are the 3D orientation (α_S,β_S) and time-to-contact t of a plane, whereas those of CDC(α,β,r) are the center (α,β) and radius r of a curvature circle. Next, the transform performed in the column of SDC(α_S,β_S,t) is a combination of the cross-ratio and polar transforms, whereas that of CDC(α,β,r) is the 3D normal-line transform.

We also point out that a VLSI implementation research (Akima et al., 2017) was reported to realize the series of cells from LGN cell to motion-detection cell (Figure 19) using electric circuit and to detect a local image motion in each RF.

5.4.1.3. Hypothesis of cell-array conversions across the visual cortex.

Based on the two sub-hierarchies in Figure 19 (which are shown as the green and red rectangles (Section 5.4.1.1) and as the blue rectangles (Section 5.4.1.2), respectively), we give below the generalized description of the cell-array conversions that was mentioned at the beginning of Section 5.4.1.

As described preliminarily above (Section 5.4.1), each sub-hierarchy performs a series of cell-array conversions: specifically, cell arrays are being converted one after another within the hierarchy; for example, an array (x,y) of LGN cells is converted to the array (ρ,θ) of NDS simple cells (see Figure 6(B)(ii and iii)), and such array conversion continues within the hierarchy. These array conversions are concretely described, as follows: in the first sub-hierarchy, each cell array is converted in the order (x,y), (ρ,θ), (α,β,r), and r (or (α,β)); in the second sub-hierarchy, each cell array is converted in the order (ρ,θ,τ), (θ,τ), (τ_X,τ_Y), and (α_S,β_S,t) (or (α_S,β_S,d)). In addition, cells more later within each sub-hierarchy acquire more complex features. These array conversions are suggested to play an important role in acquiring complex features: this suggestion will be verified later in this section.

We have found that each array conversion is performed by one of three types of operation that are convolution, correlation, and pooling (or accumulation or positive-component accumulation), which is shown in Figure 19. A representation of what array conversion each operation performs is shown, as follows, independent of individual cell arrays. First, the convolution converts an array (a,b) into the array (c,d) or (c,d,e) to create all elements as new parameters: we note that only DOG convolution performed by the cell LGN(x,y) does not create new parameters because its DOG filter has a local weight matrix (Kawakami and Okamoto, 1996; Kawakami, 1996). Second, the correlation converts an array (a,b) into the array (a,b,c) to create a new parameter c that represents this correlation. Third, the pooling converts an array (a,b,c) to the array (a,b) to annihilate a parameter c: we note that only the positive-component accumulation (i.e. a type of pooling), performed by the cell $CDC_{\alpha,\beta}$(r) in Figure 19(A), converted the array (α,β,r) into the array (r) to annihilate a parameter (α,β) that has two variables of α and β.

In this way, the convolution and correlation creates new parameters (i.e. new features) to acquire more complex feature: this acquisition has allowed the above suggestion of "these array conversions play an important role in acquiring complex features" to be verified. On the other hand, the pooling annihilates an array parameter to acquire the invariance (or constancy) for this parameter. These are interesting features of the array conversions (or the operations).

Examples of these creation and annihilation of parameters are described as follows. First, the convolution, performed by the cell CDC(α,β,r) in Figure 19(A), converts the array (ρ,θ) into the array (α,β,r) to create new parameters (α,β,r). Next, the spatio-temporal correlation (i.e. a type of correlation), performed by the cell SC_{DS}(ρ,θ,τ) in Figure 19(B), converts the array (ρ,θ) into the array (ρ,θ,τ) to create a new parameter τ that represents this correlation. Finally, the positive-component accumulation (i.e. a type of pooling), performed by the cell CDC_r(α,β) in Figure 19(A), converts the array (α,β,r) into the array (α,β) to annihilate a parameter r.

The above is summarized as follows, and gives a generalized description: (1) each sub-hierarchy performs a series of cell-array conversions; (2) each array conversion is performed by one of convolution, correlation, and pooling; (3) the convolution and correlation create new array parameters (i.e. new features) to acquire more complex feature, whereas the pooling annihilates an array parameter to acquire the invariance to that parameter; (4) thus, this array conversion allows every cell in the hierarchy to acquire either more complex feature or the invariance (or the constancy); (5) each of the 10 cell types in this hierarchy performs a cell-array conversion inherent to it, and thus the hierarchy is composed of 10 types of cell array-conversion.

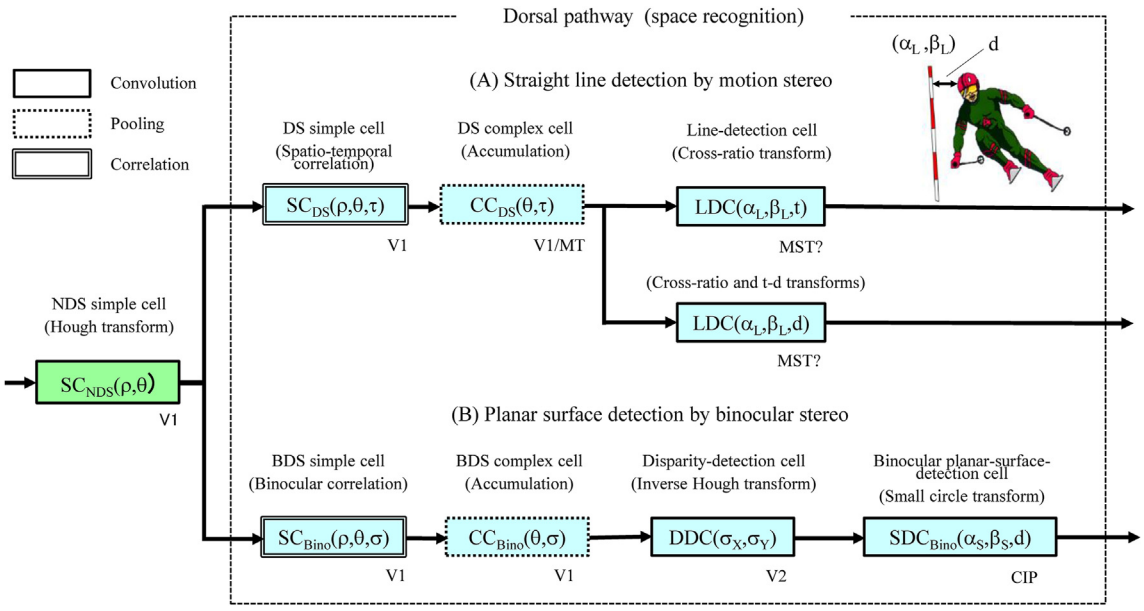

Figure 20. Two types of cell hierarchy related to space recognition. The cell $SC_{NDS}(\rho,\theta)$ shown as the green rectangle is the same as in Figure 19, and is also connected with two types of cell hierarchy in (A) and (B). (A) This hierarchy, which detects a spatial information of straight lines by motion stereo, was previously modeled (Sugie et al., 2006; Sugie, 2007), as follows, where the cells $SC_{NDS}(\rho,\theta)$, $SC_{DS}(\rho,\theta,\tau)$, and $CC_{DS}(\theta,\tau)$ are the same as in Figure 19. The line-detection cell denoted as $LDC(\alpha_L,\beta_L,t)$ (or $LDC(\alpha_L,\beta_L,d)$) integrates responses of the cells $CC_{DS}(\theta,\tau)$ over all RFs on the eyeball to detect the spatial information of a straight line. This information is composed of the time-to-passage t (or the shortest distance d) to the line and its 3D orientation (α_L,β_L), respectively: specifically, this time t (or distance d) represents the time until the line will reach just right beside (or the shortest distance when the line will come just right beside). This cell was modeled as the cross-ratio transformation (or as a combination of the cross-ratio and t-d transformations) of the cell responses $CC_{DS}(\theta,\tau)$, respectively: this cell can also be modeled as a convolution between the cell responses $CC_{DS}(\theta,\tau)$ and a synaptic weight matrix that represents the cross-ratio transform (or the above combination). Using this spatial information, we can do a slalom of ski as follows: predicting the time t and distance d to the pole (i.e. the vertical straight line) allows us to ski so as to pass very close to the pole without hitting it. (B) This hierarchy, which detects a spatial information of planes by binocular stereo, was previously modeled (Kawakami, 1996; Kawakami et al., 1999, 2010), as follows. First, a series of cells (i.e. the BDS simple, BDS complex, and disparity-detection cells) was modeled using the binocular correlation, accumulation, and inverse Hough transform, respectively, to detect a 2D disparity (σ_X,σ_Y) in each RF. Next, a binocular planar-surface-detection cell denoted as $SDC_{Bino}(\alpha_S,\beta_S,d)$ integrates these disparities (σ_X,σ_Y) over all RFs on the eyeball to detect the spatial information of a plane. This information is composed of the 3D orientation (α_S,β_S) of the plane and the shortest distance d to it; this distance d is normalized by the distance between the left and right eyes (Kawakami et al., 2010). This cell $SDC_{Bino}(\alpha_S,\beta_S,d)$ was modeled as the small-circle transformation of the cell responses $DDC(\sigma_X,\sigma_Y)$: this cell can also be modeled as a convolution between the cell responses $DDC(\sigma_X,\sigma_Y)$ and a synaptic weight matrix that represents the small-circle transform. We point out that this series of transforms above is the same as that in Figure 19(B) that are based on motion stereo: this is because the binocular disparity is mathematically equivalent to the motion disparity, which was shown in Figures. 19 and 22 of Kawakami et al. (2010) and Figure 6.2-1 of Kawakami (1996). We also point out that based on this mathematical equivalence between the binocular and motion parallaxes, binocular stereo allows the spatial information (i.e., the 3D orientation (α_L,β_L) and the shortest distance d) of a straight line to be detected: specifically, the motion stereo algorithm of Figure 20(A) (i.e. the spatio-temporal correlation, the accumulation, and the combination of the cross-ratio and t-d transforms) can be used to detect that information. Thus, based on this algorithm, we can model the cells that detect this information by binocular stereo.

This nature of the sub-hierarchies suggest that such array conversion is commonly performed by various cell types in the visual cortex to acquire either the complex feature or the invariance. Therefore, we propose a hypothesis that this array conversion is one of the basic functions across this cortex. This array-conversion hypothesis is supported not only by the two sub-hierarchies in Figure 19, but also by the following two hierarchies of cell models shown in Figure 20: the first is the cell hierarchy for detecting straight lines in space with motion stereo, and the second is the cell hierarchy for detecting planes in space with binocular stereo.

5.4.2. Hierarchies supporting the array-conversion hypothesis

5.4.2.1. Cell hierarchy for detecting straight lines in space with motion stereo.

This hierarchy (Figure 20(A)) is the first hierarchy supporting the above array-conversion hypothesis: it allows the spatial information of straight lines to be detected with motion stereo.

This hierarchy was previously modeled (Sugie et al., 2006; Sugie, 2007), where the cells $SC_{NDS}(\rho,\theta)$, $SC_{DS}(\rho,\theta,\tau)$, and $CC_{DS}(\theta,\tau)$ are the same as in Figure 19. A line-detection cell denoted as $LDC(\alpha_L,\beta_L,t)$ (or $LDC(\alpha_L,\beta_L,d)$) detects the spatial information of a straight line. This information is composed of three types of line parameter: the time-to-passage t and shortest distance d to the line and its 3D orientation (α_L,β_L), where the details of the time t and distance d are described in the caption of Figure 20(A).

This hierarchy has the following same two properties as those described in Section 5.4.1.3, thus supporting the array-conversion hypothesis above: (1) this hierarchy performs a series of cell-array conversions, specifically, each cell array is converted in the order (ρ,θ,τ), (θ,τ), and (α_L,β_L,t) (or (α_L,β_L,d)), thus being converted one after another within the hierarchy; (2) each array conversion is performed by one of convolution, correlation, and pooling.

This hierarchy plays an important role in space recognition, specifically, using the spatial information above, we, including animals, can perform actions to avoid the environment and actions to adapt to it. First, we can do a slalom of ski as follows (see the picture of doing slalom in Figure 20 (A)): predicting the time t and distance d to the pole (i.e. the vertical straight line) allows us to ski so as to pass very close to the pole without hitting it. Next, in daily life, the obstacle avoidance using this spatial information is performed as follows: this prediction to an obstacle such as a pillar (which is also a vertical line) allows us to avoid the pillar to the direction orthogonal to its orientation (α_L,β_L); also, this prediction

to the step of stair (which is a horizontal line) allows us to go up the stairs by straddling the step to a direction orthogonal to its orientation (α_L,β_L). Finally, animals also use this prediction as follows: in the jumping of an equestrian competition, this prediction to the obstacle bar allows a horse to jump over it; also, this prediction to branches (i.e. straight lines) in the forest, which are crowded in various orientations in space, allows wild birds to fly around while avoiding these branches quickly.

This cell LDC(α_L,β_L,t) uses the same column as the cell CDC(α,β,r) in Figure 6 (C), which is similar to in Section 5.4.1.2. The difference between them lies in the column parameters (in this case, the 3D orientation (α_L,β_L) and time-to-passage t of the line) and the transform performed in the column (in this case, the cross-ratio transform).

Neither neurophysiological nor psychological reports on these cells LDC(α_L,β_L,t) and LDC(α_L,β_L,d) has yet been made. Since these cell types detect the same types of spatial information (i.e. the time, shortest distance, and 3D orientation) as the SDC, they are assumed to be in area MST as well as the SDC.

5.4.2.2. Cell hierarchy for detecting planes in space with binocular stereo.

This hierarchy (Figure 20(B)) is the second hierarchy supporting the above array-conversion hypothesis: it allows the spatial information of planes to be detected with binocular stereo. This hierarchy were previously modeled, as follows.

A series of cells from the binocular-disparity selective (BDS) simple cell to the disparity-detection cell detects a two-dimensional (2D) disparity (σ_X, σ_Y) in each RF (Kawakami, 1996; Kawakami et al, 1992, 1999; Okamoto and Kawakami, 1992; Kawakami and Okamoto, 1992). Then, by integrating this disparity (σ_X, σ_Y) for all RFs on the eyeball, a binocular planar-surface-detection cell denoted as SDC_{Bino}(α_S,β_S,d) detects the spatial information of a plane (Kawakami et al., 2010; Okamoto, 2006). This information is composed of two types of plane parameter: the shortest distance d to the plane and its 3D orientation (α_S,β_S).

This hierarchy has the following same two properties as those described in Section 5.4.1.3, thus supporting the array-conversion hypothesis above: (1) this hierarchy performs a series of cell-array conversions, specifically, each cell array is converted in the order (ρ,θ,σ), (θ,σ), (σ_X,σ_Y), and (α_S,β_S,d), thus being converted one after another within the hierarchy; (2) each array conversion is performed by one of convolution, correlation, and pooling.

This hierarchy plays important roles in space recognition, as follows. First, the above spatial information allows us to perceive the distance d to a plane and its 3D orientation (α_S,β_S) without moving (or without moving the head): on the other hand, the cell SDC(α_S,β_S,d) based on motion stereo (Figure 19(B)) does not enable this information to be detected because it is stationary. Second, the spatial information of planes that were hidden in a random dot stereogram (RDS) was detected by this cell SDC_{Bino}(α_S,β_S,d) (Okamoto, 2006; Kawakami et al., 2010). This detection has allowed the psychological finding of Julesz (1960, 1971) to be explained neurophysiologically: Julesz found that one can detect the information hidden in the RDS with binocular stereo.

This cell SDC_{Bino}(α_S,β_S,d) uses the same column as the cell CDC(α,β,r) in Figure 6 (C), which is similar to in Section 5.4.1.2. The difference between them lies in the column parameters (in this case, the 3D orientation (α_S,β_S) and shortest distance d) and the transform performed in the column (in this case, the small-circle transform).

This hierarchy reflects the response to various stimuli in actual cells, as follows: (1) responses of the cells SC_{Bino}(ρ,θ,σ) and CC_{Bino}(θ,σ) are consistent with those of BDS simple cells (Poggio and Ficsher, 1977; Ohzawa et al., 1990: Freeman and Ohzawa, 1990) and BDS complex cells (Ohzawa et al., 1990) in area V1, respectively; (2) responses of the cells DDC(σ_X, σ_Y) and SDC_{Bino}(α_S,β_S,d) are consistent with those of disparity-detection cells in area V2 (Hubel & Livingston, 1987, 1990; Poggio et al., 1988) and cells in the caudal intra-parietal area (CIP) of monkeys (Tsutsui et al., 2002), respectively.

5.4.3. Summary of the cell-array conversions

The four types of cell hierarchy, in which the cell-array conversions are performed, were described in Figures 19 and 20: the first is the hierarchy from the LGN cell to the cell $CDC_{\alpha,\beta}$(r) (or CDC_r(α,β)) in Figure 19; the second, third, and fourth are shown in Figures 19(B), 20(A), and (B), respectively.

These hierarchies are composed of 16 types of cell, each of which was modeled by an inherent network that was implemented by neuron's synaptic functions, specifically, by the postsynaptic excitation, postsynaptic inhibition, and synaptic transmission efficiency. In these hierarchies, the following eight types of cell detect the shape and space informations: (1) the three types of CDC (i.e. CDC(α,β,r), $CDC_{\alpha,\beta}$(r), and CDC_r(α,β)), which detect shape information and are shown as red rectangles; (2) five types of cell (i.e. SDC(α_S,β_S,t), SDC(α_S,β_S,d), LDC(α_L,β_L,t), LDC(α_L,β_L,d), and SDC_{Bino}(α_S,β_S,d)), which detect space information and are shown as blue rectangles.

We found that these hierarchies had the following noteworthy natures. First, each hierarchy performs a series of cell-array conversions. Second, each array conversion is performed in one of three types of operation that are convolution, correlation, and pooling. Classifying these operation types of them, the largest number is 10 for convolution, followed by 4 for pooling, and the lowest for 2 for correlation. Third, the convolution and correlation create new array parameters (i.e. new features) to acquire more complex feature, whereas the pooling annihilates an array parameter to acquire the invariance to that parameter. Fourth, thus, this array conversion allows every cell in the hierarchy to acquire either more complex feature or the invariance (or the constancy).

Therefore, we also found that these four hierarchies are composed of 16 types of cell-array conversion across various areas of the visual cortex, specifically, across areas LGN, V1, V2, V4, MT, MST, FEF, and CIP. It is surprising that these areas performing the array conversions occupy the majority of the visual cortex. This supports the array-conversion hypothesis that was proposed in Section 5.4.1.3 as "this array conversion is one of the basic functions across the visual cortex". We believe that a higher-order recognition that integrates shape and space recognitions, which are essential to our daily life, is performed based on these array conversions.

Riesenhuber and Poggio (1999) described the function of convolution (i.e. template match) as "a template match is a neural transfer function suitable for increasing feature complexity". This function is consistent with that described above as "the convolution creates new array parameters (i.e. new features) to acquire more complex features".

We think that the area IT cells at the end of the ventral pathway are not regularly arranged unlike these 16 cell types, and thus can not perform these cell-array conversions. This is because if area IT has the cell array as described above, this array requires a huge number of cells (or array parameters or array dimensions) in order to represent abstract object categories like faces and hands. Thus, another representation different from this cell array is required in area IT. Instead of this array representation where each cell represents a feature, we propose a new representation where each closed loop composed of some cells represents a feature. This representation may allow the above abstract categories to be represented. This is because each cell is used in common for many loops, so that a relatively small number of cells can form a large number of loops; thus, many loops that are required for representing the abstract categories can be formed using so not many cells.

Further, each hierarchy in Figures 19 and 20 consists of the feedforward systems, in which the cell arrays and the networks connecting the cells are fixed. With these fixed feedforward systems, it is difficult to recognize complex features, including an increased complexity due to environmental changes. We think that area IT may perform a feedback system that can adapt to changes in the environment and update itself: the above closed loop, composed of some cells, may implement a kind of feedback system.

6. Conclusion

The contour of an arbitrary figure can be represented as a group of curvature circles in contact with the contour (Figure 1(A)), with each curvature circle represented by its center O_C and radius r. This representation allows the contour composed of points to be converted into a set of the centers O_C and radii r of these curvature circles. To achieve this conversion, we found an algorithm for detecting each curvature circle (Section 2), specifically, we found the algorithm performing a 3D normal-line transform for detecting the circle: this transform is one of the main points of this paper.

Based on this algorithm, we modeled a series of cells that detected the O_C and r of the circle (Figure 6; Section 3). This series was composed of an LGN cell, NDS simple cell, and CDC. The LGN and NDS simple cells were previously modeled using the DOG convolution and Hough transform, respectively.

This CDC was modeled using the above 3D normal-line transform (Figure 6), as follows. Each tangent in contact with this circle was detected by an NDS simple cell that performed the Hough transformation of LGN cell responses. Then, this normal-line transform causes the NDS simple cell to activate all CDCs on a 3D normal line within the CDC column. Finally, performing this normal-line transform for all tangents caused a CDC at the intersection of these normal lines to fire most intensively (Figure 4(B)), and thus the center O_C and radius r of the circle were detected as the coordinates of this intersection.

Therefore, this CDC was modeled as the 3D normal-line transformation of NDS simple cell responses to detect the circle. The CDC can be also modeled as a convolution between the NDS simple cell responses and a synaptic weight matrix that represents the network performing this transform.

This CDC detects every curvature circle constituting the above contour, and thus allows the contour to be converted into a set of the centers O_C and radii r of these circles (Section 3.1). In other words, the CDCs detecting all curvature circles allow the contour to be converted into the evolute of it that is constituted by this set (Section 2): this conversion is similar to Fourier transform. No cell model that detects the center and radius of this circle has been reported except for this CDC, as far as we know. The CDC can detect both the entire circle and its part (i.e. its circular arc).

This CDC has three features (Section 3.4). The first feature is its ability to process an arbitrary figure in space composed of straight lines and curves using only circles on the eyeball. The second feature is its ability for an arbitrary figure to be reconstructed by CDCs that detect all curvature circles constituting this figure. The third feature is its ability to sort and extract various components of this figure in the order of coarse-to-fine. It was clarified that these three features results from the cell arrangement of the CDC column.

Computer simulations verified the following (Section 4): (1) the CDCs correctly detected various curvature circles that constitute figures; (2) the three features described above were confirmed; (3) the network linking retinal cells and CDCs (Figure 6) functioned correctly to detect the circles.

Based on this CDC, we modeled two types of constancy CDC that have perceptual constancy (Section 3.5): a position-invariant CDC denoted as $CDC_{\alpha,\beta}(r)$ and a curvature-invariant (i.e. size-invariant) CDC denoted as $CDC_r(\alpha,\beta)$. The cell $CDC_{\alpha,\beta}(r)$ was modeled as a positive-component accumulation (i.e. a type of pooling) of the cell responses $CDC(\alpha,\beta,r)$ preferring the same r radius, and the cell $CDC_r(\alpha,\beta)$ was modeled as that preferring the same (α,β) center: note that the cell $CDC(\alpha,\beta,r)$ denotes the above CDC, and the center (α,β) of the curvature circle detected by this cell is the same as the center O_C in Figure 1(A).

Combining these two constancy CDC types with the above series of cell models (Figure 6), we formed a cell hierarchy (Figure 10; Section 3.6). This hierarchy is composed of the LGN cell, NDS simple cell, $CDC(\alpha,\beta,r)$, $CDC_{\alpha,\beta}(r)$, and $CDC_r(\alpha,\beta)$, and is functionally composed of a series of mathematical transforms: the DOG convolution, Hough transform, 3D normal-line transform, and two types of positive-component accumulation. Each transform represents a network that connects the front and back adjacent cell arrays, and is implemented by synaptic functions of neurons. Thus, this hierarchy was modeled using the operations that can be implemented with neuron's synaptic functions.

The series of cells constituting this hierarchy, to our knowledge, has been systematically modeled in the neurophysiological processes for the first time, including the modeling of their networks performing these transforms.

These three CDC types were compared with actual cells in area V4 (Section 5.1). As a result, the following correspondences were found. First, the cells $CDC_{\alpha,\beta}(r)$ and $CDC_r(\alpha,\beta)$ exhibited the same invariance and selectivity to stimuli as the position-invariant cells and curvature-invariant cells, respectively. Next, the cell $CDC_r(\alpha,\beta)$ exhibited the same preference as the cell that preferred a concentric circle. Finally, the cell $CDC(\alpha,\beta,r)$ corresponded to two types of cell: the first is the cell that responded selectively to both curvature and position of a contour; the second is the cell that exhibited a trade-off between curvature preference and position invariance. Thus, it was shown that these three CDC types reflected the response to various stimuli in actual area V4 cells.

In addition, we made the following explanations: (1) the selective-response width $\Delta_{\alpha\beta}$ of cell $CDC(\alpha,\beta,r)$ allowed the neurophysiological process why this trade-off occurs to be explained; (2) the third feature (Section 3.4) allowed the coarse-to-fine response of area IT cells to be explained neurophysiologically.

In order to validate these three CDC types neurophysiologically, we proposed three types of experimental method using microelectrodes (Section 5.3), where each method type uses a circle or dot or bar stimulus.

We made the following two comparisons with previous models (Section 5.2).

First, we compared the cell hierarchy (Figure 10) with cell models previously reported. As a result, the following correspondence and difference were found: (1) the NDS simple cell, $CDC(\alpha,\beta,r)$, and $CDC_{\alpha,\beta}(r)$ of the hierarchy corresponded to the S1, S2, and C2 cells of the above cell models, respectively; (2) this hierarchy differed most from these cell models in that the hierarchy is represented by a series of mathematical transformations that represent its networks (i.e. the Hough transform, 3D normal-line transform, and two types of positive-component accumulation).

Second, the cell $CDC(\alpha,\beta,r)$ was compared with a cell model that responds selectively to a very local curvature (i.e. a circular arc with very small central angle) and has been named an endstopped cell. As a result, the followings were found: (1) this endstopped cell can be modeled also based on the network in Figure 6, and this modeling is equivalent to performing the curvature-circle detection (Section 3.1) for this arc with very small central angle; (2) increasing this angle until an entire circle is formed allows the cell CDC (α,β,r) to be modeled.

We proposed that the cell-array conversions, which were found in Section 3.6 and played an important role in acquiring the complex feature and the constancy, are performed commonly in the visual cortex (Section 5.4). Making this proposal is another key point in our paper, and was done as follows:

First, combining the above hierarchy (Figure 10; Section 3.6) with three hierarchies modeled previously, we formed four types of hierarchy (Figures 19 and 20), which are composed of 16 types of cell model and process both shape and space informations.

Next, we found that these hierarchies had the following noteworthy natures (Section 5.4): (1) each hierarchy performs a series of cell-array conversions; (2) each array conversion is performed by one of

convolution, correlation, and pooling; (3) the convolution and correlation create new array parameters (i.e. new features) to acquire more complex feature, whereas the pooling annihilates an array parameter to acquire the invariance to that parameter; (4) thus, this array conversion allows every cell in the hierarchy to acquire either more complex feature or the invariance (or the constancy).

Finally, thus, we also found that these four hierarchies are composed of 16 types of cell-array conversion across various areas of the visual cortex, specifically, across areas LGN, V1, V2, V4, MT, MST, FEF, and CIP. It is surprising that these areas performing the array conversions occupy the majority of the visual cortex. Based on this finding, we proposed a hypothesis that such array conversions are one of the basic functions performed across the visual cortex except for area IT, and are performed commonly in the cortex to play an important role in acquiring the complex feature and the constancy. We believe that a higher-order recognition that integrates shape and space recognitions, which are essential to our daily life, is performed based on these array conversions.

Declarations

Author contribution statement

All authors listed have significantly contributed to the development and the writing of this article.

Funding statement

This research did not receive any specific grant from funding agencies in the public, commercial, or not-for-profit sector.

Competing interest statement

The authors declare no conflict of interest.

Additional information

Supplementary content related to this article has been published online at https://doi.org/10.1016/j.heliyon.2020.e05397.

Acknowledgements

We thank Yuki Sugie for his support with the programing about the simulator, and Kazuhiro Sakamoto for his suggestions regarding physiology.

References

Akima, H., Kawakami, S., Madrenas, J., Moriya, S., Yano, M., Nakajima, K., Sakuraba, M., Sato, S., 2017. Complexity reduction of neural network model for local motion detection in motion stereo vision. In: International Conference on Neural Information Processing (ICONIP) 2017, pp. 830–839.

Bar, M., 2003. A cortical mechanism for triggering top-down facilitation in visual object recognition. J. Cognit. Neurosci. 15, 600–609.

Blasdel, G.G., 1992. Orientation selectivity, preference, and continuity in monkey striate cortex. J. Neurosci. 12, 3139–3161.

Bronshtein, I.N., Semendyayev, K.A., 1978. Handbook of Mathematics. Van Nostrand Reinhold Company.

Cadieu, C., Kouh, M., Riesenhuber, M., Poggio, T., 2004. Shape Representation in V4: Investigating Position-specific Tuning for Boundary Conformation with the Standard Model of Object Recognition. CBCL Paper 241/AI Memo 2004–024. MIT, Cambridge, MA, 2004.

Cadieu, C., Kouh, M., Pasupathy, A., Connor, C.E., Riesenhuber, M., Poggio, T., 2007. A model of V4 shape selectivity and invariance. J. Neurophysiol. 98, 1733–1750.

Chen, T., Chung, K., 2001. An efficient randomized algorithm for detecting circles. Comput. Vis. Image Understand. 83, 172–191.

De Marco, T., Cazzato, D., Leo, M., Distante, C., 2015. Randomized circle detection with isophotes curvature analysis. Pattern Recogn. 48, 411–421.

Desimone, R., Albright, T.D., Gross, C.G., Bruce, C., 1984. Stimulusselective properties of inferior temporal neurons in the macaque. J. Neurosci. 4, 2051–2062.

Duda, R.O., Hart, P.E., 1972. Use of the Hough transformation to detect lines and curves in pictures. Comm. Assoc. Comput. 15, 11–15.

Dumoulin, S.O., Hess, R.F., 2007. Cortical specialization for concentric shape processing. Vis. Res. 47, 1608–1613.

El-Shamayleh, Y., Pasupathy, A., 2016. Contour curvature as an invariant code for objects in visual area V4. J. Neurosci. 36, 5532–5543.

Felleman, D.J., Van Essen, David C., 1991. Distributed hierarchical processing in the primate cerebral cortex. Cerebr. Cortex 1, 1–47.

Freeman, R.D., Ohzawa, I., 1990. On the neurophysiological organization of binocular vision. Vis. Res. 30, 1661–1676.

Fujita, I., Tanaka, K., Ito, M., Cheng, K., 1992. Columns for visual features of objects in inferotemporal cortex. Nature 360, 343–346.

Fujiwara, K., Akao, T., Kawakami, S., Fukushima, J., Kurkin, S., Fukushima, K., 2014. Neural correlates of time-to-collision estimation from visual motion in monkeys. Equilib. Res. 73, 144–153.

Gallant, J.L., Braun, J., Van Essen, D.C., 1993. Selectivity for polar, hyperbolic, and cartesian gratings in macaque visual cortex. Science 259, 100–103.

Gallant, J.L., Connor, C.E., Rakshit, S., Lewis, J.W., Van Essen, D.C., 1996. Neural responses to polar, hyperbolic, and cartesian gratings in area V4 of the macaque monkey. J. Neurophysiol. 76, 2718–2739.

Gibson, J.J., 1950. The Perception of the Visual World. Houghton Muffin.

Gibson, J.J., 1979. The Ecological Approach to Visual Perception. Houghton Mifflin, 1979.

Hashimoto, M., 2009. A Research of Shape Representation in Higher Visual Cortex (Master's Thesis). Tohoku University, Sendai, Japan (in Japanese).

Hegde, J., Van Essen, D.C., 2000. Selectivity for complex shapes in primate visual area V2. J. Neurosci. 20, 1–6.

Hubel, D.H., Wiesel, T.N., 1959. Receptive fields of single neurons in the cat's striate cortex. J. Physiol. 148, 574–591.

Hubel, D.H., Wiesel, T.N., 1962. Receptive fields, binocular interaction and functional architecture in the cat's visual cortex. J. Physiol. 160, 106–154.

Hubel, D.H., Wiesel, T.N., 1965. Receptive fields and functional architecture in two nonstriate visual areas (18 and 19) of the cat. J. Neurophysiol. 28, 229–289.

Hubel, D.H., Wiesel, T.N., 1968. Receptive fields and functional architecture of monkey striate cortex. J. Physiol. 195, 215–243.

Hubel, D.H., Livingstone, M.S., 1987. Segregation of form, color, and stereopsis in primate area 18. J. Neurosci. 7, 3378–3416.

Hubel, D.H., Livingstone, M.S., 1990. Color and contrast sensitivity in the lateral geniculate body and primary visual cortex of the macaque monkey. J. Neurosci. 10, 2223–2237.

Hughes, H.C., Nozawa, G., Kitterle, F., 1996. Global precedence, spatial frequency channels, and the statistics of natural images. J. Cognit. Neurosci. 8, 197–230.

Hung, C.P., Kreiman, G., Poggio, T., DiCarlo, J.J., 2005. Fast readout of object identity from macaque inferior temporal cortex. Science 310, 863–866, 2005.

Illingworth, J., Kittler, J., 1987. The adaptive Hough transform. IEEE Trans. Pattern Anal. Mach. Intell. 5, 690–698.

Ito, M., Tamura, H., Fujita, I., Tanaka, K., 1995. Size and position invariance of neuronal responses in monkey inferotemporal cortex. J. Neurophysiol. 73, 218–226.

Ito, M., Komatsu, H., 2004. Representation of angles embedded within contour stimuli in area V2 of macaque monkeys. J. Neurosci. 24, 3313–3324.

Ito, M., Goda, N., 2011. Mechanisms underlying the representation of angles embedded within contour stimuli in area V2 of macaque monkeys. Eur. J. Neurosci. 33, 130–142.

Ito, T., 2011. A Study on a Neural Network Model for Morphological Expression Using Curvature (Master's Thesis). Tohoku University, Sendai, Japan (in Japanese).

Jones, J.P., Palmer, L.A., 1987. The two-dimensional spatial structure of simple receptive fields in cat striate cortex. J. Neurophysiol. 58, 1187–1211.

Julesz, B., 1960. Binocular depth perception of computer-generated patterns. Bell Syst. Tech. J. 39, 1125–1162.

Julesz, B., 1971. Stereoscopic vision. Vis. Res. 26, 1601–1612.

Kawakami, S., Okamoto, H., Morita, T., 1992. A model for intracortical connections of hypercolumn 3: correlation filterings and direction selectivity cells. Technical Report NC92-13 of the IEICE, pp. 89–96 (in Japanese).

Kawakami, S., Okamoto, H., 1992. A model for intracortical connections of hypercolumn 6: circle detection cell and connections of prestriate cells. Technical Report NC92-47 of the IEICE, pp. 21–28 (in Japanese).

Kawakami, S., 1996. A Study on a Neural Network Model for the Detection of Local Image Motion on the Visual Cortex (Doctoral dissertation). Tohoku University, Sendai, Japan (in Japanese).

Kawakami, S., Okamoto, H., 1996. A cell model for the detection of local image motion on the magnocellular pathway of the visual cortex. Vis. Res. 36, 117–147.

Kawakami S., Yasukawa, Y., Hasegawa, F., Inamoto, Y., Morita, T. Okamoto, H. (1999). Process and Apparatus for Extracting and Recognizing Figure Elements Using Division into Receptive fields, Polar Transformation, Application of One-Dimensional Filter, and Correlation between Plurality of Images. United States Patent, 5901252.

Kawakami, S., Matsuoka, M., Okamoto, H., Hosogi, S., 2000. A Neural Network Model for Detecting Planar Surface Spatially from the Optical Flow in Area MST of the Visual Cortex. Transaction J83-D-II of the IEICE, pp. 2786–2797 (in Japanese).

Kawakami, S., Matsuoka, M., Okamoto, H., Hosogi, S., 2002. A neural network model performing spatial recognition on the visual cortex: why it looks three-dimensional with one eye when it moves ? J. Soc. Instrum. Control Eng. 41, 744–748 (in Japanese).

Kawakami, S., Matsuoka, M., Okamoto, H., Hosogi, S., 2003. A neural network model for detecting a planar surface spatially from the optical flow in area MST of the visual cortex. Syst. Comput. Jpn. 34, 2786–2797.

Kawakami S., Matsuoka M., Okamoto H. & Hosogi S. (2010). Image Measurement Method, Image Measurement Apparatus and Image Measurement Program Storage media. European Patent Application, EP2148304A2.

Kobatake, E., Tanaka, K., 1994. Neuronal selectivities to complex object features in the ventral visual pathway of the macaque cerebral cortex. J. Neurophysiol. 71, 856–867.

Kuffler, S., Nicholls, J.G., Martin, A.R., 1984. From Neuron to Brain. Sinauer Assoc, Sunderland.

Lee, D.N., Reddish, P.E., 1981. Plummeting gannets: a paradigm of ecological optics. Nature 293, 293–294.

Liu, R.F., Niu, Y.Q., Wang, S.R., 2008. Thalamic neurons in the pigeon compute distance-to-collision of an approaching surface. Brain Behav. Evol. 72, 37–47.

Logothetis, N.K., Pauls, J., Poggio, T., 1995. Shape representation in the inferior temporal cortex of monkeys. Curr. Biol. 5, 552–563.

Nandy, A.S., Sharpee, T.O., Reynolds, J.H., Mitchell, J.F., 2013. The fine structure of shape tuning in area V4. Neuron 78, 1102–1115.

Ohzawa, I., DeAngelis, G.,C., Freeman, R.D., 1990. Stereoscopic depth discrimination in the visual cortex: neurons ideally suited as disparity detectors. Science 249, 1037–1041.

Okamoto, H., Kawakami, S., 1992. A model for intracortical connections of hypercolumn 4: disparity selectivity cells. Technical Report NC92-14 of the IEICE, pp. 97–104 (in Japanese).

Okamoto, H., Kawakami, S., Saito, H., Hida, E., Odajima, K., Tamanoi, D., Ohno, H., 1999. MT neurons in the macaque exhibited two types of bimodal direction tuning as predicted by a model for visual motion detection. Vis. Res. 39, 3465–3479.

Okamoto, H., 2006. A Study on a Neural Network Model Performing Motion Stereo on the Visual Cortex (Doctoral Dissertation). Tohoku University, Sendai, Japan (in Japanese).

Oleskiw, T.D., Nowack, A., Pasupathy, A., 2018. Joint coding of shape and blur in area V4. Nat. Commun. 9, 1–13.

Pasupathy, A., Connor, C.E., 1999. Responses to contour features in macaque area V4. J. Neurophysiol. 82, 2490–2502.

Pasupathy, A., Connor, C.E., 2001. Shape representation in area V4: position-specific tuning for boundary conformation. J. Neurophysiol. 86, 2505–2519.

Pasupathy, A., Connor, C.E., 2002. Population coding of shape in area V4. Nat. Neurosci. 5, 1332–1338.

Perrett, D., Rolls, E., Caan, W., 1982. Visual neurons responsive to faces in the monkey temporal cortex. Exp. Brain Res. 47, 329–342.

Poggio, G.F., Ficsher, B., 1977. Binocular interaction and depth sensitivity in striate and prestriate cortex of behaving rhesus monkey. J. Neurophysiol. 40, 1392–1405.

Poggio, G.F., Gonzalez, F., Krause, F., 1988. Stereoscopic mechanisms in monkey visual cortex: binocular correlation and disparity selectivity. J. Neurosci. 8, 4531–4550.

Riesenhuber, M., Poggio, T., 1999. Hierarchical models of object recognition in cortex. Nat. Neurosci. 2, 1019–1025.

Rodriguez-Sanchez, A.J., Tsotsos, J.K., 2012. The roles of endstopped and curvature tuned computations in a hierarchical representation of 2D Shape. PloS One 7, 1–13.

Roe, A.W., Chelazzi, L., Connor, C.E., Conway, B.R., Fujita, I., Gallant, J.L., Lu, H., Vanduffel, W., 2012. Toward a unified theory of visual area V4. Neuron 74, 12–29.

Rust, N.C., DiCarlo, J.J., 2010. Selectivity and tolerance ("invariance") both increase as visual information propagates from cortical area V4 to IT. J. Neurosci. 30, 12978–12995.

Schiller, P.H., Finlay, B.L., Volman, S.F., 1976. Quantitative studies of single-cell properties in monkey striate cortex: 1. Spatiotemporal organization of receptive fields. J. Neurophysiol. 39, 1288–1319.

Schneider, R., Riesenhuber, M., 2002. Translation Invariance in a Hierarchical Neural Model of Visual Object Recognition. AI Memo, 2002-011.

Serre, T., Wolf, L., Bileschi, S., Riesenhuber, M., Poggio, T., 2007. Robust object recognition with cortex-like mechanisms. IEEE Trans. Pattern Anal. Mach. Intell. 29, 411–426.

Sharpee, T.O., Kouha, M., Reynolds, J.H., 2013. Trade-off between curvature tuning and position invariance in visual area V4. PNAS (Proc. Natl. Acad. Sci.) 110, 11618–11623.

Stanislas, D., 2003. The neural basis of the Weber–Fechner law: a logarithmic mental number line. Trends Cognit. Sci. 7, 145–147.

Sugase, Y., Yamane, S., Ueno, S., Kawamoto, K., 1999. Global and fine information coded by single neurons in the temporal visual cortex. Nature 400, 869–873.

Sugie, Y., Kawakami, S., Sakamoto, K., Yano, M., 2006. A cell model for detecting the time-to-passage of a line. Jpn Neural Network Soci. Magaz. 13, 146–147 (in Japanese).

Sugie, Y., 2007. A Cell Model for Detecting Time-To-Passage of a Line (Master's Thesis). Tohoku University, Sendai, Japan (in Japanese).

Tamura, H., Tanaka, K., 2001. Visual response properties of cells in the ventral and dorsal parts of the macaque inferotemporal cortex. Cerebr. Cortex 11, 384–399.

Tanaka, K., Saito, H., Fukada, Y., Moriya, M., 1991. Coding visual images of objects in the inferotemporal cortex of the macaque monkey. J. Neurophysiol. 66, 170–189.

Tanaka, K., 1996. Inferotemporal cortex and object vision. Annu. Rev. Neurosci. 19, 109–139.

Tsao, D.Y., Freiwald, W.A., Tootell, R.B.H., Livingstone, M.S., 2006. A cortical region consisting entirely of face-selective cells. Science 311, 670–674.

Tsutsui, K., Sakata, H., Naganuma, T., Taira, M., 2002. Neural correlates for perception of 3D surface orientation from texture gradient. Science 298, 409–412.

Ungerleider, L.G., Mishkin, M., 1982. Two cortical visual systems. In: Ingle, D.J., Goodale, M.A., R.J.W. (Eds.).

Wagner, H., 1982. Flow-field variables trigger landing in flies. Nature 297, 147–148.

Wang, Y., Frost, B.J., 1992. Time to collision is signaled by neurons in the nucleus rotundus of pigeons. Nature 356, 236–238.

Wörgötter, F., Eysel, U.T., 1989. Axis of preferred motion is a function of bar length in visual cortical receptive fields. Exp. Brain Res. 76, 307–314.

Xu, L., Oja, E., Kultanen, P., 1990. A new curve detection method: randomized Hough transform (RHT). Pattern Recogn. Lett. 11, 331–338.

Zoccolan, D., Kouh, M., Poggio, T., DiCarlo, J.J., 2007. Trade-off between object selectivity and tolerance in monkey inferotemporal cortex. J. Neurosci. 27, 12292–12307.